ADVANCED OPTICAL MATERIALS
www.advopticalmat.de

Empowered Layer Effects and Prominent Properties in Few-Layer Metasurfaces

Shuqi Chen, Yuebian Zhang, Zhi Li, Hua Cheng, and Jianguo Tian*

Metamaterials are 3D artificial structures proposed to surpass conventional natural materials and realize novel functions beyond traditional optical elements. Nevertheless, they are usually bulky and difficult to be fabricated. As 2D equivalents of metamaterials, metasurfaces have been proposed to overcome the drawbacks of metamaterials and fully control the polarization, amplitude, phase, and dispersion of electromagnetic waves. Relative to single-layer metasurfaces that have limited controllability and functionality, few-layer metasurfaces have more degrees of freedom and abundant layer effects to design novel devices and achieve high-efficiency applications. This review is focused on the empowered layer effects and prominent properties in few-layer metasurfaces, and some distinctive applications proposed in recent years are discussed. It is expected that few-layer metasurfaces will provide a promising road toward the novel intelligent photonic devices, multifunctional devices, and integrated photonic devices.

1. Introduction

With the development of modern optics, traditional optical elements, such as refractive lenses and birefringent crystals, can no longer satisfy the growing requirements for intelligentialize, miniaturization, and integration in modern photonic systems. As 3D artificial substitutes for conventional natural materials, metamaterials can realize functions far beyond traditional optical devices. They are composed of periodic subwavelength artificial nanostructures that function as "electromagnetic meta-atoms" and can produce distinctive physical properties unavailable in natural materials.[1,2] Numerous remarkable applications have been realized based on the metamaterials, such as negative index materials,[3] invisibility cloaks,[4] and zero-index materials.[5] Nevertheless, metamaterials are usually bulky, difficult to be fabricated, and suffer from high energy losses, which hinder their practical applications in modern photonic systems. In recent years, planar metasurfaces, the 2D equivalents of metamaterials, have attracted plenty of attentions due to their extraordinary abilities in controlling the polarization, amplitude, phase, and dispersion of electromagnetic waves.[6–8] Compared with bulk metamaterials, the metasurfaces have many advantages, such as ultrathin thicknesses, low losses, ease of fabrication and integration. Over the past years, single-layer metasurfaces have been widely applied in realizing polarization conversion,[9] beam deflectors,[10,11] metalenses,[12,13] holograms,[14] coding,[15] structural colors,[16,17] nonlinear metasurfaces,[18] and some other applications. Nevertheless, the interactions between lights and ultrathin single-layer metasurfaces are usually limited, resulting in low efficiency and limited controllability in some applications.[19] Moreover, the degrees of freedom for light manipulation provided by a single-layer metasurface are usually not enough in realizing multifunctional devices and some other sophisticated photonic systems.

Few-layer metasurface that contains more than one functional layer provides an effective method to overcome the drawbacks of both bulk metamaterials and single-layer metasurfaces. Cheng et al. employed the concept of few-layer metasurfaces to discuss the advantages and emergent functionalities of them in ref. [20]. Few-layer metasurfaces retain the advantages of single-layer metasurfaces and can provide more degrees of freedom to manipulate electromagnetic waves. More importantly, the abundant layer effects, such as the multiple wave interference between layers and the near-field coupling effects, can enhance the interactions between lights and structures and improve the efficiency of few-layer systems. In addition, the combination of different functional layers can produce novel functions that single-layer metasurfaces can hardly realize. For example, by breaking the mirror symmetry along the propagation direction, few-layer metasurfaces can realize asymmetric transmission of linearly polarized lights.[21] By vertically integrating different metasurfaces on one substrate, optical systems with different functions can be miniaturization and integration. Recently, the few-layer metasurfaces have also been extended in the acoustic fields to realize some novel applications, such

Prof. S. Chen, Dr. Y. Zhang, Dr. Z. Li, Prof. H. Cheng, Prof. J. Tian
The Key Laboratory of Weak Light Nonlinear Photonics
Ministry of Education
School of Physics and Teda Applied Physics Institute
Nankai University
Tianjin 300071, China
E-mail: schen@nankai.edu.cn
Prof. S. Chen, Prof. H. Cheng, Prof. J. Tian
Renewable Energy Conversion and Storage Center
Nankai University
Tianjin 300071, China
Prof. S. Chen, Prof. H. Cheng, Prof. J. Tian
The Collaborative Innovation Center of Extreme Optics
Shanxi University
Taiyuan, Shanxi 030006, China
The ORCID identification number(s) for the author(s) of this article can be found under https://doi.org/10.1002/adom.201801477.

DOI: 10.1002/adom.201801477

as the wave branching effects,[22] flat Fresnel lens,[22] asymmetric transmission,[23] and valley topological phases.[24] Hence, the few-layer metasurfaces provide a promising route to novel functional devices, multifunctional devices, and integrated photonic devices.

In this paper, we focus on the basic layer effects and distinctive properties in few-layer metasurfaces, and summarize some distinctive applications proposed in recent years. In Section 2, we briefly introduce four basic mechanisms in constructing few-layer metasurfaces. In Section 3, we review some distinctive applications of few-layer metasurfaces in amplitude manipulation, polarization manipulation, phase manipulation, multidimensional manipulation of electromagnetic waves, and some multifunctional devices. In the last section, we give a brief conclusion and provide an outlook on the future development of few-layer metasurfaces.

2. Empowered Layer Effects in Few-Layer Metasurfaces

2.1. Near-Field Coupling Effects

Near-field coupling is considered from the perspective of the interactions between electric and/or magnetic resonances as shown in **Figure 1**a. For plasmonic single-layer metasurfaces, the couplings between electric resonances are relatively easy to be achieved; for example, Fano resonance can be formed by the coupling between different electric resonance modes.[25–27] However, the couplings between electric and magnetic resonances are difficult to be achieved. As a result, many novel phenomena, such as optical chirality, are hard to be realized within single-layer plasmonic metasurfaces.[28,29] The reason is that most of the plasmonic single-layer metasurfaces cannot provide magnetic resonance modes. On the other hand, for a few single-layer metasurfaces that can simultaneously support electric and magnetic resonances, such as split ring resonators (SRRs), the two resonances are perpendicular to each other, which results in the lacking of coupling. Nevertheless, the couplings between electric and magnetic resonances can be efficiently realized by few-layer metasurfaces. One method is to excite electric and magnetic resonances with parallel components through the coupling between adjacent layers.[30] The other approach is to replace the magnetic resonance with an electric resonance at the equiphase plane by controlling the space between layers.[31,32]

High-efficiency reflective metasurfaces can be achieved with the help of near-field coupling effects in the metal–insulator–metal (MIM) configuration.[33–37] This type of metasurface typically consists of a metal subwavelength resonator and a metal ground plane separated by a thin dielectric spacer. When the two metal layers are close enough, strong near-field coupling can induce antiparallel electrical currents and form a magnetic resonance inside the structure. Such resonance mode is often called as gap-plasmon mode at optical frequencies.[7,8] By changing the geometric parameters of the subwavelength resonators, full 2π phase range with near-unit reflection amplitude can be achieved. Based on this configuration, many high-efficiency reflective phase gradient metasurfaces, such as surface wave couplers[33] and broadband anomalous reflector,[34] have been proposed. It should be noticed that the MIM configuration can also realize perfect absorber by proper structural design.[38,39]

High transmittance can also be achieved by Huygens' surfaces configuration based on few-layer metasurfaces. By adjusting the surface electric and magnetic polarizabilities (α_e^{eff} and α_m^{eff}) of the few-layer metasurfaces, the reflection can

Shuqi Chen is a professor at the Key Laboratory of Weak Light Nonlinear Photonics, Ministry of Education, School of Physics and Teda Institute of Applied Physics, Nankai University, China. He received his joint training Ph.D. degree from the University of Arizona, USA, and Nankai University, China, in 2009. He was a winner of New Century Excellent Talents Support Program of the Ministry of Education of China in 2013 and Natural Science Foundation of Tianjin for Distinguished Young Scientists in 2018. His current research interests include nonlinear optics, phononic and acoustic metasurfaces, and subwavelength electromagnetics.

Yuebian Zhang is a doctoral candidate student at the Key Laboratory of Weak Light Nonlinear Photonics, Ministry of Education, School of Physics and Teda Institute of Applied Physics, Nankai University, China. He received his bachelor's degree in applied physics from Inner Mongolia University of Science & Technology in 2015. His current research focuses on nanophotonics.

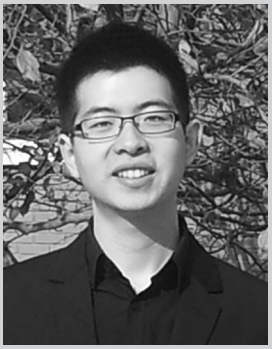

Zhi Li is a doctoral candidate student at the Key Laboratory of Weak Light Nonlinear Photonics, Ministry of Education, School of Physics and Teda Institute of Applied Physics, Nankai University, China. He received his bachelor's degree in materials physics from Nankai University in 2015. His current research focuses on nonlinear nanophotonics.

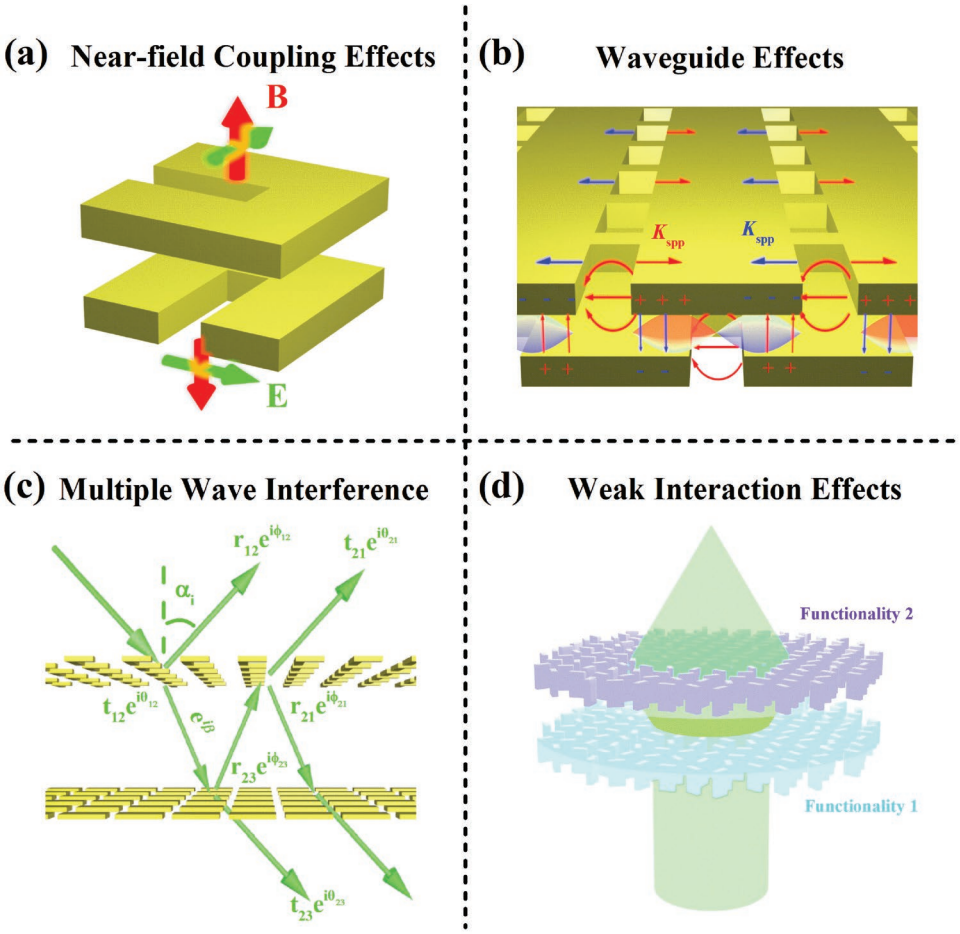

Figure 1. Four empowered layer effects in few-layer metasurfaces. a) Schematic representation of various near-field coupling effects between electric and/or magnetic resonances. b) Schematic view of waveguide effects between layers with laterally translated nanoapertures. c) Schematic of the multiple wave interference effects between two metasurface layers. d) Schematic of cascaded optical system based on weak interaction effects between layers of few-layer metasurfaces.

be completely eliminated. Then, the electric sheet admittance ($\bar{\bar{Y}}_{es} = j\omega\bar{\bar{\alpha}}_e^{eff}$) and the magnetic sheet impedance ($\bar{\bar{Z}}_{ms} = j\omega\bar{\bar{\alpha}}_m^{eff}$) can be directly extracted from the complex reflection (R) and transmission (T) coefficients:[40]

$$Y_{es} = \frac{2(1-T-R)}{\eta(1+T+R)}, \quad Z_{ms} = \frac{2\eta(1-T+R)}{(1+T-R)} \tag{1}$$

where $\eta = \sqrt{\mu/\varepsilon}$ is the wave impedance of free space. The amplitude of the transmission coefficient of each meta-atom becomes unity when the normalized electric sheet admittance and magnetic sheet impedance are purely imaginary and equal. Besides, by tuning the magnitude of the impedance, the transmitted phase can achieve any value between $-\pi$ to π. According to the above analysis, Huygens' surfaces configurations based on few-layer metasurfaces have been implemented in both microwave range[40] and near-infrared (NIR) range.[41,42]

Besides the Huygens' surfaces configuration, another widely used structure that can realize high transmittance is the ABA type few-layer metasurface, where A and B represent two ultrathin metasurface layers.[43–45] This type of metasurface can support the electromagnetic wave tunneling phenomenon under certain conditions, which can be explained by the effective medium theory. The high transmission of this kind of metasurface is always related to the high magnetic fields inside the structure. By utilizing the near-field coupling effects between different layers, one can generate effective "magnetic responses" to match the impedance. Based on this idea, many high-efficiency few-layer metasurfaces have been proposed.[46]

2.2. Waveguide Effects

The manipulation of polarization and phase of electromagnetic waves is a vital task of metasurfaces. Nevertheless, single-layer ultrathin transmissive metasurfaces cannot provide full control over the phase of the copolarized transmitted light.[19] On the other hand, although the phase of the cross-polarized transmitted light can be tuned from 0 to 2π by utilizing the Pancharatnam–Berry (PB) phase of circularly polarized light, the polarization state of transmitted light is fixed and cannot be simultaneously manipulated.[7] According to the theroy of PB phase, when a circularly polarized light is incident on an anisotropic nanoantenna, the phase of the converted circularly

polarized light can be changed by spatially rotating the unit cell. The phase change can be written as $\Phi = 2\sigma\theta$, where θ is the angle of rotation of the antenna, $\sigma = \pm 1$ represents the left-handed circular polarized (LCP) or right-handed circular polarized (RCP) lights, respectively. Therefore, the sign of the phase gradient is locked with the polarization of the incident light.[47,48] In addition, although the phase gradient of the PB metasurfaces is independent of the wave frequency, the efficiencies can be strongly frequency-dependent, dictated by the scattering properties of constitutional meta-atoms forming the metasurfaces.[47] Recently, a novel mechanism for forming waveguide mode between layers has been proposed based on few-layer metasurfaces capable of simultaneously manipulating the polarization and phase of transmitted wave.[49] This waveguide mechanism can work for both linearly polarized light and circularly polarized light. As shown in Figure 1b, surface plasmon polaritons (SPPs) can be excited at each of the metal–dielectric interfaces under normal incidence when the light is polarized perpendicular to the major axis of the rectangular metal nanoapertures. Since the coupling between the two metal layers can form a standing wave of the SPPs, a MIM waveguide can be constituted as a result. The waveguide mode makes the amplitude and phase of the transmission light sensitive to the geometrical parameters and the relative positions of the nanoapertures. In the aligned case, the phase shifting can cover a large range (about $3\pi/2$) by tuning the aperture length. By adjusting the lateral translation between the two layers, the range of phase shifting can be further extended due to a phase difference close to π existing between the aligned and laterally translated states, which can be verified by the charge oscillations at the bottom nanoapertures exhibiting opposite directions. It should be noticed that the proposed method does not need to convert the incident linearly polarized light to its cross-polarized transmitted light, which is different from many existing designs employing anisotropic resonators. For circularly polarized incident light, only the light with polarization perpendicular to the major axis of the nanoapertures can be transmitted. As a result, the polarization states of the transmitted light can be manipulated by just rotating the rectangular nanoapertures. In addition, the rotation of each unit cell can introduce an extra Berry phase term of $e^{i\theta}$ to the transmitted light, where θ is the angle of rotation. Therefore, the polarization and phase of the transmitted wave can be controlled by either aligned or laterally translated state of the few-layer metasurface. Based on this mechanism and similar structures, bidirectional perfect absorbers and generation of vector beams with arbitrary spatial variation of phase can also be realized.[50,51]

2.3. Multiple Wave Interference Effects

Compared with single-layer ultrathin metasurfaces, which are usually inefficient, a prominent advantage of few-layer metasurfaces is the existence of multiple wave interference between the functional layers, which can be used to cancel the undesired light and enhance the efficiency of the metasurfaces. Based on this method, many high efficiency devices have been demonstrated, such as antireflection-coating,[52,53] linear polarization convertor,[54] asymmetric transmission metasurfaces,[55] and metalens.[56] In general, the bottom structured layers in these metasurfaces usually act as reflectors to repeatedly reflect the incident lights. If the distances between layers are far enough so that the near-field coupling or magnetic resonance can be neglected, the reflection and transmission response of the few-layer metasurfaces can be directly obtained with multiple wave interference formula.[52,57] More specifically, if a few-layer metasurface only contains two functional layers, which are separated with a distance d, we can model the two functional layers as tuned impedance interfaces with effectively zero thickness. The overall field reflection and transmission coefficients of this metasurface can be written as

$$r = \frac{r_{12}e^{i\phi_{12}} - r_{12}r_{21}r_{23}e^{i(\phi_{12}+\phi_{21}+\phi_{23}+2\beta)} + t_{12}r_{23}t_{21}e^{i(\theta_{12}+\phi_{23}+\theta_{21}+2\beta)}}{1 - r_{21}r_{23}e^{i(\phi_{21}+\phi_{23}+2\beta)}} \tag{2}$$

$$t = \frac{t_{12}t_{23}e^{i(\theta_{12}+\theta_{23}+\beta)}}{1 - r_{21}r_{23}e^{i(\phi_{21}+\phi_{23}+2\beta)}} \tag{3}$$

where variables illustrated in Figure 1c indicate their meanings. The complex propagation phase $\beta = Nk_0d$ when the incident angle $\alpha_i = 0$. k_0 is the wavenumber in a vacuum, and N is the complex refractive index of the spacer. r_{ij} and t_{ij} are the polarization-dependent reflection and transmission coefficients at individual interfaces, which can be derived from numerical simulations of the isolated functional layers. If there are more than two stacked functional layers in a few-layer metasurface, we can still obtain the overall response of the metasurfaces by simple semi-analytical S-matrix multiplication.[58] One typical phenomenon related to multiple wave interference is the Fabry–Pérot (FP) resonance. The constructive or destructive interference can be easily achieved by forming a FP like cavity between different layers.[53–56,59] Hence, by adjusting the interference between layers, we can easily enhance the interaction between light and metasurfaces, and realize numerous efficient applications.

2.4. Weak Interaction Effects

Various novel phenomena and functionalities have been realized by using near-field interactions between layers in few-layer metasurfaces; however, most of these few-layer metasurfaces can only work in a single frequency band. The working band can be extended by the weak interaction effect between layers of few-layer metasurfaces. One way is to introduce the defect to weaken the strength of the coupling between the layers. Besides, the defect can play a certain role in manipulating the property of each layer, such as amplitude and phase.[60,61] The other method is by delicately designing, so that all layers contribute together in each working band or functionalities, while each layer dominates a single working band or functionalities.[62] Furthermore, cascaded optical system can also be realized based on weak interaction effect between layers of few-layer metasurfaces. As shown in Figure 1d, we can realize a focusing metalens and an aperture metalens in different layers and combine them together to build a cascaded optical system. The metalenses capable of eliminating various aberrations have been demonstrated by using this design strategy.[63–65]

3. Prominent Applications in Few-Layer Metasurfaces

3.1. Total Control of Amplitude and Spectrum

Few-layer metasurfaces can provide plenty of degrees of freedom to tailor their reflection, transmission, and absorption properties. The abundant interlayer effects also give the researchers more approaches to manipulate the spectral response of metasurfaces, which have been using to realize numerous excellent applications in amplitude and spectrum manipulation. In this section, we mainly discuss the asymmetric transmission devices, circular dichroism (CD), and some other selected important applications among them.

3.1.1. Asymmetric Transmission

Asymmetric transmission refers to a phenomenon that the transmission intensities of forward and backward propagating lights are different.[66–72] The forward transmission of coherent light through a metasurface can be related to the complex Jones matrix (also called *T*-matrix)

$$T^f = \begin{bmatrix} A & B \\ C & D \end{bmatrix} \tag{4}$$

where the four *T*-matrix components *A*, *B*, *C*, and *D* are complex numbers and this expression is applicable in any orthogonal basis. According to the reciprocity theorem, the complex Jones matrix of the backward propagating lights is

$$T^b = \begin{bmatrix} A & -C \\ -B & D \end{bmatrix} \tag{5}$$

The asymmetric transmission for a given base vector is determined by the difference between the off-diagonal elements of the *T*-matrix. The condition for the occurrence of asymmetric transmission is $|B| \neq |C|$. The *T*-matrix components obey fixed relations for certain symmetries. For example, in the linear base, if a structure possesses mirror symmetries with respect to a plane perpendicular to the propagation direction, we have $B = C$, and no asymmetric transmission occurs.[21,66] Therefore, the asymmetric transmission of linearly polarized light usually needs to break the mirror symmetry of a structure, which is hard to implement by using single-layer metasurfaces.

To realize the asymmetric transmission of linearly polarized light, Menzel et al. proposed a few-layer metasurface composed of chiral structures without any rotational symmetry,[66] as shown in **Figure 2**a. It consists of two layers, the upper layer comprises an L-shaped antenna and the lower one comprises a nanorod. The L-shaped antenna is used to produce the needed polarization conversion and the nanorod breaks the remaining mirror symmetry in the propagation direction. From Figure 2b,c, we can clearly observe the asymmetric transmission of linearly polarized light. In addition, this structure can also realize asymmetric transmission of circularly polarized light due to the chirality of the L-shaped antenna. However, the value for the asymmetric transmission of this metasurface can only reach 25% under linearly polarized light incidence. In fact, by carefully designing the geometry and manipulating the resonances of the structures, few-layer metasurfaces can readily realize high-efficient asymmetric transmission. Mutlu et al. proposed a few-layer metasurface that can realize high-efficient asymmetric transmission of linearly polarized waves with a measured asymmetry factor of 0.91 in the microwave range.[67] By utilizing the near-field coupling effects and electromagnetic wave tunneling phenomenon in the stacked metallic layers, the measured transmission efficiency for the backward propagating waves can reach 96% and the backward-to-forward transmission contrast can reach 19.6. The phase difference between the transmitted eigenwaves can be controlled by tailoring the subwavelength mesh sandwiched between two chiral layers. As a result, the cross-polarized transmission can be maximized in one direction and the transmission in the opposite direction can be blocked simultaneously. Besides the efficiency problem, the working bandwidths of asymmetric transmission devices also need to be considered in practical application. To address this problem, some broadband asymmetric transmission metasurfaces have been proposed in both the microwave range[73] and the NIR range.[71,74–76] Zhang et al. proposed a metasurface that can realize high-efficient, broadband, and angular robust asymmetric transmitting of linearly polarized waves.[75] It consists of three layers of gold nanogratings, which can be viewed as linear polarizers that transmit light polarized orthogonal to the grating. However, different from traditional polarizers, the transmission efficiency of the metasurface can break the Malus' law and reach 80% in experiment due to the strong multiple reflections between layers and the polarization conversion effect of the nanogratings.

Besides the asymmetric transmission of linearly polarized light, the asymmetric transmission of circularly polarized light is also required in many practical applications. To realize this effect, Pfeiffer et al. proposed a bianisotropic metasurface that consists of three patterned gold layers,[70] as shown in Figure 2d. The metasurface is designed by first finding the sheet admittances of each layer needed for a specified Jones matrix, and then finding the physical realization according to the frequency-selective surface theory. The measured *T*-matrix components of the metasurface are shown in Figure 2e,f. A maximum transmission of 50% and an extinction ratio of 20:1 can be achieved at NIR wavelengths. The relatively high efficiency can be attributed to the interference enhancement effect of the desired polarization and the suppression of the undesired polarization in transmission waves. It should be noticed that, although the asymmetric transmission phenomenon usually requires the existence of polarization conversion, it is possible to realize asymmetric transmission of the same polarization.[77,78] Figure 2g shows an asymmetric transmission device composed of alternative Ag and SiO_2 thin layers and a pair of sub-wavelength gratings.[78] The device of wavelength-scale thickness can realize asymmetric transmission of transverse-magnetic (TM) polarized visible light under normal incidence. The alternative Ag and SiO_2 thin layers between the two gratings can be viewed as a planar hyperbolic metamaterial that can act as a pass-band filter for high spatial frequencies exceeding the diffraction limit, as shown in Figure 2h. When the light is normally incident from side A on the top grating,

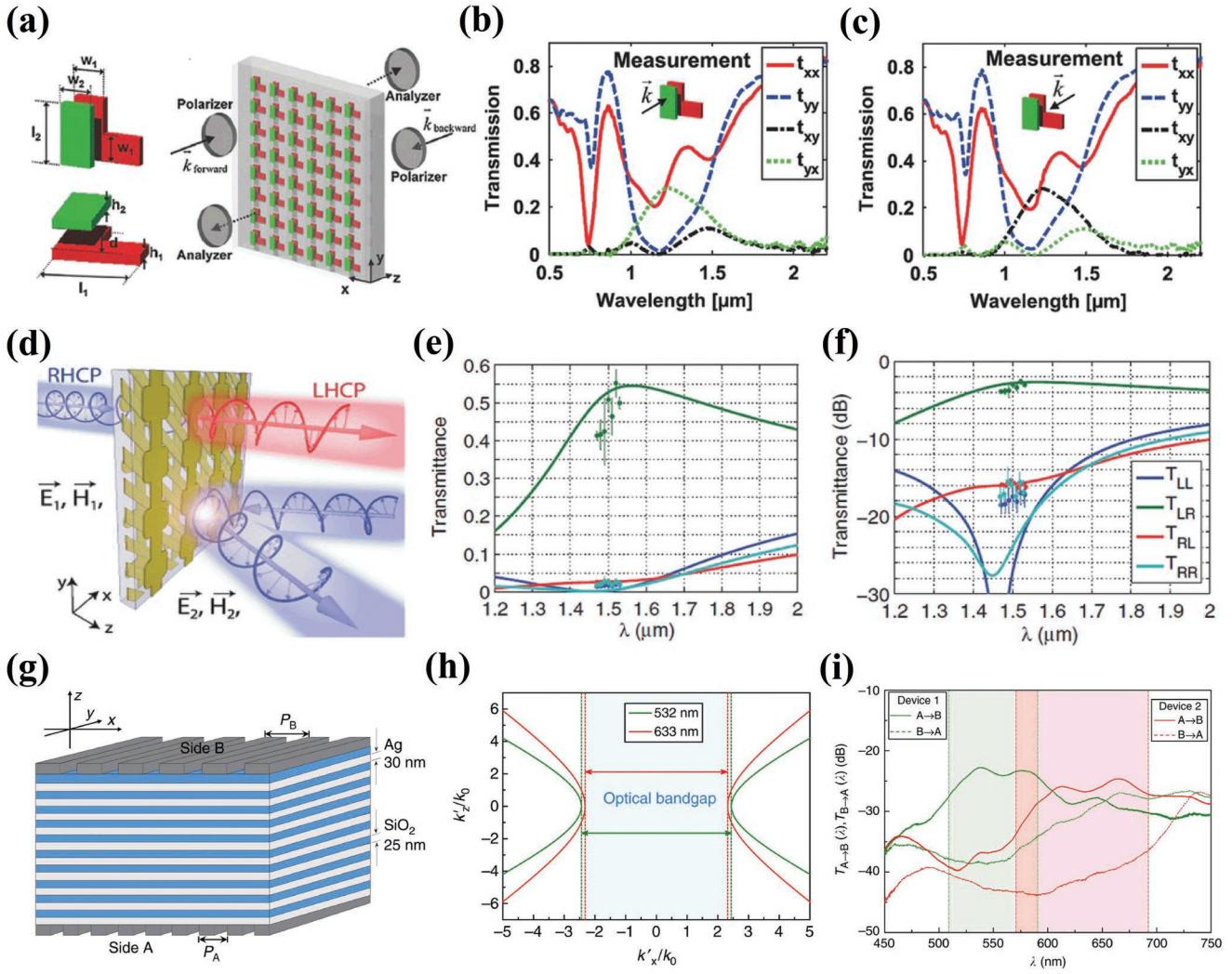

Figure 2. Asymmetric transmission. a) Schematics of the few-layer metasurface, which enables asymmetric transmission of linearly polarized waves. Measured squared moduli of the four *T*-matrix components for b) forward (+z direction) propagation and c) backward (−z direction) propagation, respectively. (a)–(c) Reproduced with permission.[66] Copyright 2010, American Physical Society (APS). d) Schematic of the few-layer metasurface, which enables asymmetric transmission of circularly polarized waves. Measured (circles) and simulated (solid lines) *T*-matrix components of the metasurface on e) linear and f) logarithmic scales. (d)–(f) Reproduced with permission.[70] Copyright 2014, APS. g) Schematic of the asymmetric transmission device composed of alternative Ag and SiO_2 thin layers. h) Dispersion relations of the asymmetric transmission device for TM polarization. i) Measured intensity transmission coefficients for two fabricated devices. (g)–(i) Reproduced with permission.[78] Copyright 2014, Nature Publishing Group (NPG).

it can excite a pair of oblique, laterally counter-propagating modes that can pass through the device with the help of the bottom grating. However, when the backward propagating light is incident from side B on the bottom grating, it is coupled to a pair of nonpropagating, evanescent modes located within the bandgap of the hyperbolic metamaterial. As a result, broadband efficient asymmetric transmission can be achieved, as shown in Figure 2i. As discussed above, few-layer metasurfaces have many prominent advantages in realizing asymmetric transmission of electromagnetic waves compared with single-layer metasurfaces. Although there exist some difficulties in realizing high-efficiency and broadband asymmetric transmission in the visible region due to the Ohmic losses of plasmonic structures, these problems can hopefully be solved by using dielectric materials.[79]

3.1.2. Optical Chirality

Chirality is a ubiquitous geometrical phenomenon in the natural world, which refers to lacking any mirror-image symmetry of an object.[80] Fascinating optical effects caused by chirality can also be found in various biological species. For example, single network gyroid biophotonic crystals have been proved that can produce vivid structural colors of butterfly wings,[81] helicoidal structures of the beetle elytra make *Chrysina gloriosa* possess a brilliant metallic appearance under LCP illumination.[82] These intriguing effects mainly arise from the different response of optical chiral materials to LCP and RCP waves and can be roughly divided into two major categories, optical rotation (OR) and CD. OR is caused by the difference in refractive index between LCP and RCP waves of a chiral material,

resulting in the rotation of polarization when linearly polarized light passes through the material. While the difference in the absorbance for LCP and RCP waves of a chiral material leads to CD. Chirality is also an important property for biological and chemical researchers. It exists widely in biomacromolecules, thus the detection of optical chiral response of molecules is an effective approach to explore their spatial configurations. However, the chirality of natural material is generally subtle, so a long light–matter interaction length is required, otherwise it is hard to be discriminated. Compared with naturally occurring chiral materials, few-layer metasurfaces have shown the ability to significantly enhance the optical chiral responses, which in turn provide a promising way for biochemical conformation and structural analysis.[28,29,83] Similar to the natural molecules, few-layer metasurfaces can generate intrinsic chirality, which is an inherent property and not subjected to external conditions. Besides the universal OR and CD effects, novel phenomenon can also be generated by few-layer metasurfaces, such as negative refractive indices as shown in **Figure 3**a,b.[30,84–86]

The existence of geometric chirality for nanostructures is not equal to the existence of optical chiral responses, but it is still a good starting point for research. It has been proved that the CD signal is derived from the Coulomb interaction between nanoparticles,[87] thus the spectrum mainly depends on the geometry and composition of the nanostructures, and the symmetry of a frame is very important for forming a strong chiral response for this type of few-layer metasurfaces.[88–90] As shown in Figure 3c, only configurational optical chiral response emerges if similar meta-atoms are arranged in a handed fashion because resonant plasmonic coupling is an essential prerequisite. The insets show the enantiomers (red and blue) and the achiral nanostructures (black). The ΔT spectrum can be flipped by changing the handedness of the enantiomers and the difference in transmittance is up to 7%. However, the optical chiral response observed in this type of few-layer metasurfaces is not significant due to the fact that although the structures meet geometric chirality, it is clearly not satisfied with the requirement for optical response. In fact, it has been proved that the generation of optical chirality requires the near-field coupling of electric and magnetic fields. The constitutive relations can be described as follows for a general optical chiral medium:[91,92]

$$\vec{D} = \varepsilon_0 \overleftrightarrow{\varepsilon}_r \vec{E} + \frac{i\overleftrightarrow{\chi}}{c_0}\vec{H} \tag{6}$$

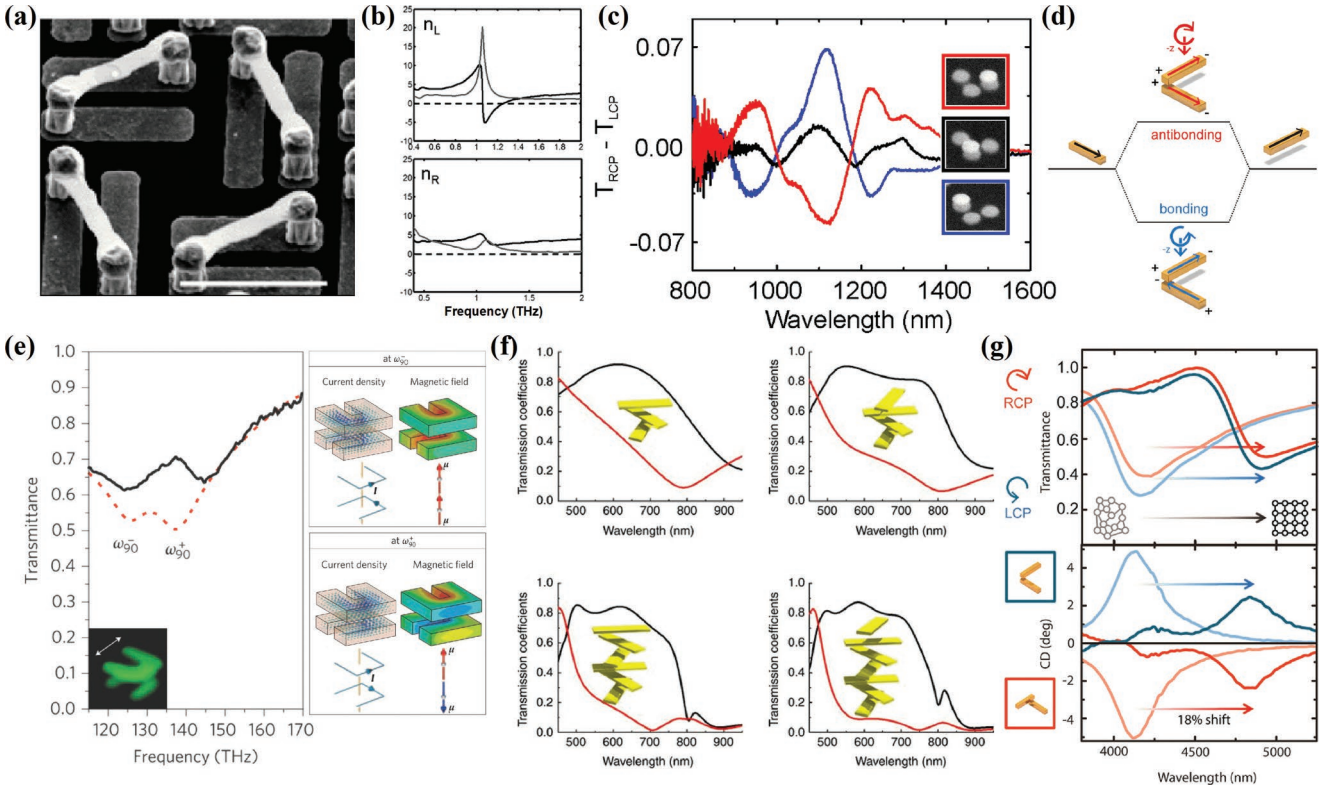

Figure 3. Optical chirality realized by few-layer metasurfaces. a) Scanning electron microscopy (SEM) image of the chiral few-layer metasurface. b) The experimentally retrieved real (black) and imaginary (gray) parts of refractive index under LCP and RCP waves, respectively. (a,b) Reproduced with permission.[30] Copyright 2009, APS. c) Experimental $\Delta T_{LCP–RCP}$ spectra. Insets: SEM images of meta-atoms with different handedness. Reproduced with permission.[88] Copyright 2012, American Chemical Society (ACS). d) Schematic of the hybridization model for chiral plasmonic Born–Kuhn modes. Reproduced with permission.[104] Copyright 2013, ACS. e) Left panel: experimental transmittance spectra for 90° twisted split rings. Right panel: the numerical current and magnetic field distributions for the 90° twisted split rings. Reproduced with permission.[105] Copyright 2009, NPG. f) Simulated transmittance spectra under RCP (black) and LCP (red) illuminations with 3 to 4 and 6 to 7 layers. Insets: Illustration of the chiral metasurfaces with different layers. Reproduced with permission.[110] Copyright 2012, NPG. g) Experimental transmittance and CD spectra through the active few-layer metasurface under LCP and RCP illuminations for the amorphous (lighter curves) and crystalline (darker curves) states of phase change material. Reproduced with permission.[117] Copyright 2015, ACS.

and

$$\vec{B} = -\frac{i\overleftrightarrow{\chi}}{c_0}\vec{E} + \mu_0\overleftrightarrow{\mu}_r\vec{H} \tag{7}$$

where ε_0, μ_0, and c_0 are the permittivity, permeability, and speed of light in vacuum, respectively; and $\overleftrightarrow{\varepsilon}_r$, $\overleftrightarrow{\mu}_r$, and $\overleftrightarrow{\chi}$ are the relative permittivity, permeability, and chirality tensors, respectively. For simplicity, we consider an isotropic chiral material (the parameters in the above equations are simplified to scalars), which has different optical responses under LCP and RCP illuminations, thus the refractive indices and impedances for RCP (+) and LCP (−) waves are given by

$$n_\pm = \sqrt{\varepsilon_r\mu_r} \pm \chi \tag{8}$$

and

$$z_\pm = z_0\sqrt{\mu_r/\varepsilon_r} \tag{9}$$

where z_0 is the vacuum impedance. From Equation (8), one can readily infer that the phase difference between the two circularly polarized waves is $\mathrm{Re}(n_+ - n_-)dk_0$, where d is the thickness of the chiral material and k_0 is the wave vector in vacuum. Thus, the rotation angle of OR can be expressed as $\theta = \mathrm{Re}(\chi)dk_0$. Alternatively, the difference in transmittance is $T_\pm = \exp[-\mathrm{Im}(n_+ - n_-)dk_0]$. Furthermore, in case of a weak absorption, CD can be simplified to CD $\approx 2dk_0\mathrm{Im}(\chi)$. It is obvious that the optical chiral response can be significantly enhanced via effectively near-field coupling between electric and magnetic fields from Equations (6) to (9). In this section, we mainly discuss various few-layer metasurfaces which can generate CD. We will discuss OR in Section 3.2, together with polarization conversion, because OR is similar in phenomenon to polarization conversion.

As one representative type of chiral nanostructures, helical metal structures were theoretically proposed and experimentally demonstrated, which can introduce a set of parallel electric and magnetic components.[91,93–95] When circularly polarized light is incident on the helical structure perpendicular to the axis of rotation, both electric and magnetic dipoles can be excited and paralleled to each other, which means the resonances are effectively coupled. Thus, strong chiral response can be observed. However, helical metal structures still face the challenges of high costs and are hard to work in the visible range. Various few-layer metasurfaces that support the coupling between electric and magnetic dipoles have also been proposed to replace the helical structures.[30,96–98] These few-layer metasurfaces were primarily designed to work in the microwave and terahertz regions due to their complicated configurations. As shown in Figure 3a, the meta-atom can be equivalent to an inductor-capacitor (LC) resonant circuit, the bottom metal strips form a capacitor and the loop acts as an inductor. An electric dipole along the direction of capacitor and a magnetic dipole along the direction of inductor can always be generated simultaneously when oscillating current flows through the metal loop. Since the angle between the two dipoles is small, significant chiral response is anticipated. From Equation (8), we can find that if the chiral response χ is strong enough, the nanostructure will present a negative refractive index for one circularly polarized light. Figure 3b indicates the experimentally retrieved effective parameters of the few-layer metasurface. The real part of the refractive index for LCP wave reaches negative values due to the strong chiral response, while the refractive index for RCP wave remains positive over the whole frequency range.

Another strategy is to replace the magnetic dipole with an electric dipole, which means one electric dipole is used to mimic magnetic dipole and the other electric dipole can be coupled in different equiphase planes.[31,32] Following this strategy, a few-layer gammadion structures with a little different dimensions was proposed to exhibit CD at NIR wavelengths.[99] Apart from the dimensional inconsistency, rotating misalignment can also induce strong optical chirality, such as twisted gold crosses.[100] Due to the isotropy of the gold cross, linear birefringence can be avoid. As a consequence, the twisted gold crosses exhibit pronounced CD while the polarization conversion can be negligible. Chiral effective parameter retrieval has also been applied,[101] which shows that the strong optical chirality leads to a difference in the refractive indices for LCP and RCP waves as large as 0.35. Similar to the plasmon hybridization model,[102,103] a plasmonic analog of the Born–Kuhn model of chiral nanostructures has been used to characterize the near-filed coupling of electric dipoles, as illustrated in Figure 3d.[104] The bonding and antibonding states are generated owing to the strong coupling of the electric dipoles. Because of the favorable arrangement of charges, the bonding state is at lower energy level compared with individual nanorod while the antibonding state lies at higher energy level. By delicately adjusting the inter-rod distance, remarkable CD effect has been demonstrated based on this model. Higher degree of freedom between the electric and magnetic modes can also be realized by few-layer metasurfaces, which leads to more complex hybridization of chirality.[105] Figure 3e demonstrates a few-layer chiral metasurface of twisted split rings and its transmission spectrum can be adjusted by changing the twist angle. The numerical current and magnetic field distributions for the 90° twisted split rings are shown in the right panel of Figure 3e. Both electric and magnetic dipoles can be excited in the upper and lower SRRs. However, the electric dipoles in the slit gaps are perpendicular to each other, thus no electric dipole–dipole interaction occurs. Therefore, the resonance levels are determined by magnetic dipole–dipole coupling in the near-field. The magnetic dipoles at resonances ω_{90}^- and ω_{90}^+ are aligned parallel and antiparallel, respectively, leading to different transmittance responses. The twisted SRRs were later arranged in a fourfold rotational symmetry (C_4) supercell, which could completely eliminate polarization conversion and obtain CD effect.[106] Giant optical chiral has also been realized in a few-layer twisted-arc metasurface.[107] Moreover, the sign of the CD spectrum in a plasmonic system can also be controlled by small relative shifts between the coupled structures.[108] Two stacked L-shaped nanoantennas constitute the plasmonic system, as we discussed before, two hybridized modes are distinctly excited. As the displacement between the two nanoantennas is continuously tuned, the resonance energy of the hybridized modes relative to one another shifts. For a given energy, the sign of the CD spectrum is changed. From the perspective of the hybridization model, the lateral displacement changes the charges of the opposite/same

sign located at the coincident part, thus an inversion of the hybridization happens. The strength of the optical chirality can also be engineered within twisted nanorods.[109] The previous works were mostly dual-layer metausrfaces. Actually, the optical chiral response can be further enhanced when more layers are involved, as shown in Figure 3f.[110] Stronger optical chirality can be observed, as the number of layers increases due to the strong coupling between the closely spaced twisted nanorods. From another perspective, the working mechanism can also be understood as the extension of the dual-layer structure.

Recently, new types of chiral few-layer metasurfaces have also been demonstrated. In fact, the optical chiral response is not limited in the linear regime. This effect in second harmonic generation (SHG) is several orders of magnitude more significant than its linear counterpart.[111,112] Since SHG only exists in materials with noncentrosymmetric atomic lattice or nanostructures with no inversion symmetry, the intrinsically noncentrosymmetric chiral few-layer metasurfaces are spontaneously suitable for possessing strong SHG. Different from the linear CD effect, the sign of the CD spectra does not change by flipping the sample in the SHG process, while the normalized quantity SHG-CD signal would change which is defined as $\text{SHG-CD} = \Delta P^{2\omega}_{\text{SHG-CD}} / P^{2\omega}_{\text{ave}} = 2(P^{2\omega}_{\text{LCP}} - P^{2\omega}_{\text{RCP}})/(P^{2\omega}_{\text{LCP}} + P^{2\omega}_{\text{RCP}})$.[113] Various few-layer metasurfaces have been demonstrated to possess strong SHG-CD signals,[114,115] which has promising application prospects in chiral imaging. The concept of "handedness switching" has also been transferred from organic chemistry to chiral few-layer metasurfaces. By changing the conductivity of silicon with external optical stimuli, handedness switching in few-layer metasurfaces has been demonstrated.[116] Another approach to realize tunable and switchable chiral few-layer metasurface is to adopt phase change materials whose dielectric constant can be adjusted by external excitation such as laser pulses, voltage, or temperature.[117] The phase change material $Ge_3Sb_2Te_6$ (GST-326) was employed due to the large difference in refractive indices between amorphous and crystalline states, which can cause a large spectral shift of the resonance position. Corner-stacked nanorods were chosen as the underlying system and modified by sandwiching a layer of GST-326 between them. Figure 3g presents the tunable chirality experimental results, which shows that a giant spectral shift of 18% was realized. Few-layer metasurfaces can further provide a platform for enhancing chiral light–matter interactions such as two-photon luminescence from quantum emitters.[118] Few-layer twisted-arc metasurface was infused with achiral quantum emitters. Thanks to the confinement of the incident light around the metasurface, two-photon luminescence was remarkably chiral-selective enhanced compared with a reference case without metasurface.

3.1.3. Other Applications in Amplitude and Spectrum Manipulation

The multiple wave interference effect and near-field coupling effect between layers make the few-layer metasurface a powerful platform to tailor the reflection,[52,53,119,120] transmission,[121–127] and absorption[39,128–131] of electromagnetic waves. By utilizing the multiple wave interference effect between the functional layers, Chen et al. proposed a wide-angle antireflection coating in the terahertz frequency range.[52] The metasurface consists of arrays of gold split-ring resonators and a gold mesh, as shown in **Figure 4**a. It can be seen from Figure 4b that almost zero reflection is achieved due to the destructive interference of the multiple reflections waves in the metasurface coating. Further study shows that the antireflection coating works well over a wide range of angles of incidence for both transverse electric (TE) and TM polarizations. Recently, broadband antireflection metasurfaces operating at terahertz and mid-infrared wavelengths have been proposed based on the same mechanism.[53] The broadband character of these metasurfaces was achieved by tuning the structural geometry to bring two antireflection bands closer. Over the past few years, few-layer metasurfaces have realized many novel applications in both near-field distribution and far-field spectrum manipulation. One interesting application among them is the wave-based analog computing.[123] Figure 4c shows the cascaded optical system that can perform mathematical operations. It consists of three parts: the first part and the third part are two graded-index dielectric slabs with parabolic variation of permittivity that can perform the Fourier transform and the inverse Fourier transform, respectively; the second part is a suitably tailored metasurface spatial filter, which can either be a metasurface with prescribed permittivity and permeability or a metatransmit-array. The simulated results are shown in Figure 4d. The z-component of the electric field distribution is used as the input function. The device can produce a field profile at the output end, which is proportional to the first differentiation of the input field profile. This technique can realize some fundamental mathematical operators, such as differentiation, integration, and convolution. The far-field spectrum properties of metasurfaces are related to the near-field resonant response of the structures. In recent years, the nonradiating anapole resonance modes have attracted great interests among researchers due to their distinctive properties in reducing the radiation loss and enhancing the near-field.[132,133] However, the excitation of anapole modes is quite challenging by using single-layer metasurfaces without resorting to complex excitation configuration.[133] Recently, Wu et al. proposed a few-layer metasurface that can support anapole mode in the NIR range under normally incident plane-wave.[132] The metasurface consists of a gold film perforated by dumbbell-shaped apertures and arrays of vertical split-ring resonators (VSRRs), as shown in Figure 4e. The incident light can excite a horizontal electric dipole and a horizontal toroidal dipole around the dumbbell-shaped apertures. The VSRRs are used to enhance the toroidal dipole and suppress the undesired magnetic quadrupole. The near-field coupling effect between the top dumbbell-shaped apertures and the bottom VSRRs plays a vital role in realizing the anapole mode. Because the toroidal dipole moment has exactly the same far-field scattering pattern as the electric dipole moment, when the toroidal dipole and electric dipole are superimposed with the same amplitude but out of phase, the destructive interference of them will produce the nonradiating anapole mode with strong near-field enhancement. Figure 4f shows the measured reflection and transmission of the metasurface. A reflection dip is observed around the anapole resonance wavelength, which can be tuned by changing the gap size between the Au apertures and the VSRRs. Few-layer metasurfaces have also been applied to the realization of structural

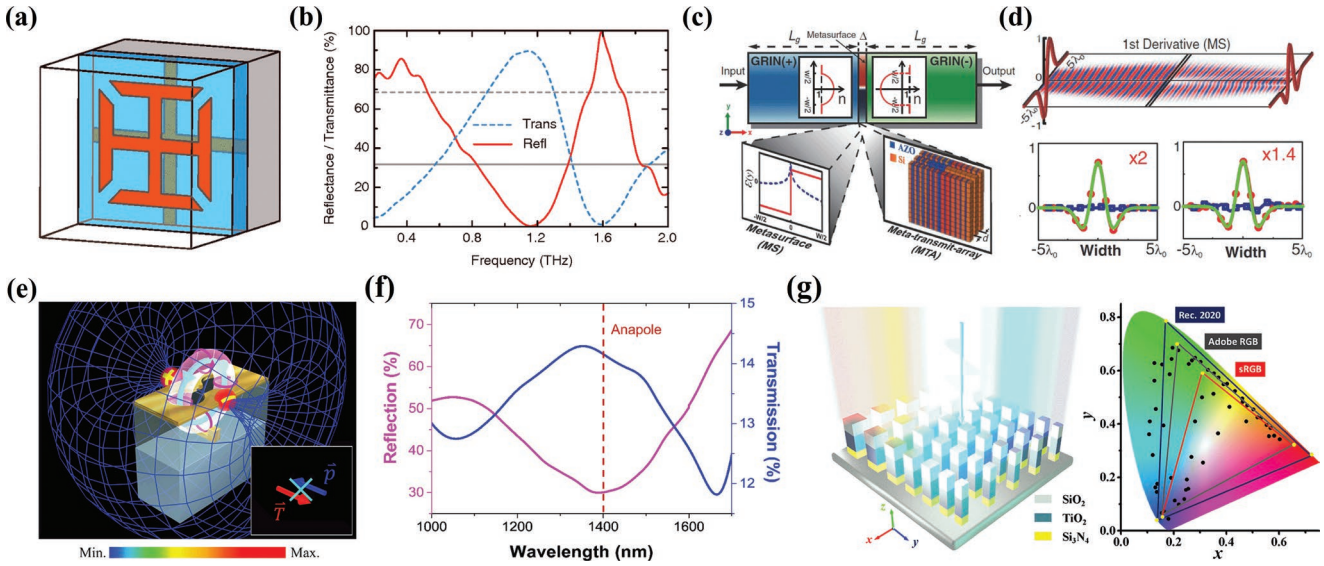

Figure 4. a) Schematic of the antireflection coating. b) Measured reflection and transmission of the antireflection coating under normal incidence. (a,b) Reproduced with permission.[52] Copyright 2010, APS. c) Schematic of the metasurface that can perform mathematical operations. d) Upper panel: perspective view of the propagation of a wave throughout the system functioning as first differentiator. The input function is shown at left and the output profile is shown at right. The snapshot shows the simulated z-component of the electric field. Lower panels: simulated results (real (red) and imaginary (blue) parts) at the output for first differentiation using different metasurfaces. The green lines are the expected analytical results. (c,d) Reproduced with permission.[123] Copyright 2014, American Association for the Advancement of Science (AAAS). e) Schematic of the metasurface that enables the excitation of the nonradiating anapole mode. f) Measured reflection and transmission of the metasurface. The red dashed line represents the simulated resonant wavelength of the anapole mode. (e,f) Reproduced with permission.[132] Copyright 2018, ACS. g) Left panel: schematic of the multidielectric metasurface that can realize ultrahigh saturation structural colors. Right panel: the corresponding CIE 1931 chromaticity coordinates based on simulated spectra for the designed samples. Reproduced with permission.[134] Copyright 2013, ACS.

colors in recent years.[17,134] By using multidielectric stacked layers, Yang et al. experimentally obtained ultrahigh saturation structural colors ranging from 70% to 90% with full hue,[134] as shown in Figure 4h. The unit cell consists of a SiO_2 capping layer, a TiO_2 spacer layer, and a Si_3N_4 bottom layer. This design strategy can deeply modulate the multipolar modes inside the structure and thus has more advantages in manipulating the spectrum responses of metasurfaces. The monochromaticity of reflection spectra can be dramatically enhanced via suppressing excitation of multipolar modes at shorter wavelength. Therefore, the saturation and color gamut space can be significantly increased. The simulated color gamut space can occupy 171% sRGB space, 127% Adobe RGB space, 126% DCI-P3 space, and 90% Rec. 2020 color space, which indicates the proposed metasurfaces are promising for high-end and advanced display applications. Above examples indicate that the few-layer metasurfaces are more flexible in manipulating the near-field properties and controlling the far-field spectrum responses than single-layer metasurfaces.

3.2. Manipulation of Polarization

Conventional methods to manipulate the polarization state of electromagnetic waves, such as magneto-optic phenomenon,[135] birefringent crystals,[136] and polarized molecules,[137] exist with the disadvantages of bulky size and narrow working bandwidth, which impose a tough challenge on the miniaturization and integration of optical systems. On the other hand, metasurfaces can directly manipulate the polarization state of electromagnetic waves at the sub-wavelength scale with a wider bandwidth. Furthermore, the polarization state of electromagnetic waves can be finely modified to the pixel scale (meta-atom) utilizing metasurfaces, thus the outputs of arbitrary polarization states can be easily realized. Compared with monolayer metasurfaces, few-layer metasurfaces have the ability to reasonably redistribute the incident energy and increase the length of light–structure interaction through multiple wave interference and near-field coupling between layers, thus the efficiency and bandwidth of polarization conversion can be effectively improved.

We will first discuss OR effect as mentioned before. Same as CD effect, OR is generated by near-field coupling of different electric and/or magnetic modes. Giant gyrotropy has been achieved in twisted rosettes through strong coupling between electric and magnetic dipoles as shown in **Figure 5**a.[138,139] This result proved that strong polarization rotatory power can be achieved not only in continuous helical structure but also in few-layer metasurfaces. The experimental results shown in Figure 5b indicate that a linearly polarized wave passing through the metasurface will be converted into elliptically polarized wave, and its polarization azimuth will rotate. The observed gyrotropy of the bilayered metasurface is several orders of magnitude stronger than the natural materials. Besides, due to the strong optical chirality, this few-layer metasurface can also generate negative refraction. The OR effects in former works exist with strong dispersion because the metasurfaces operate in resonance frequencies. By adopting a reversed

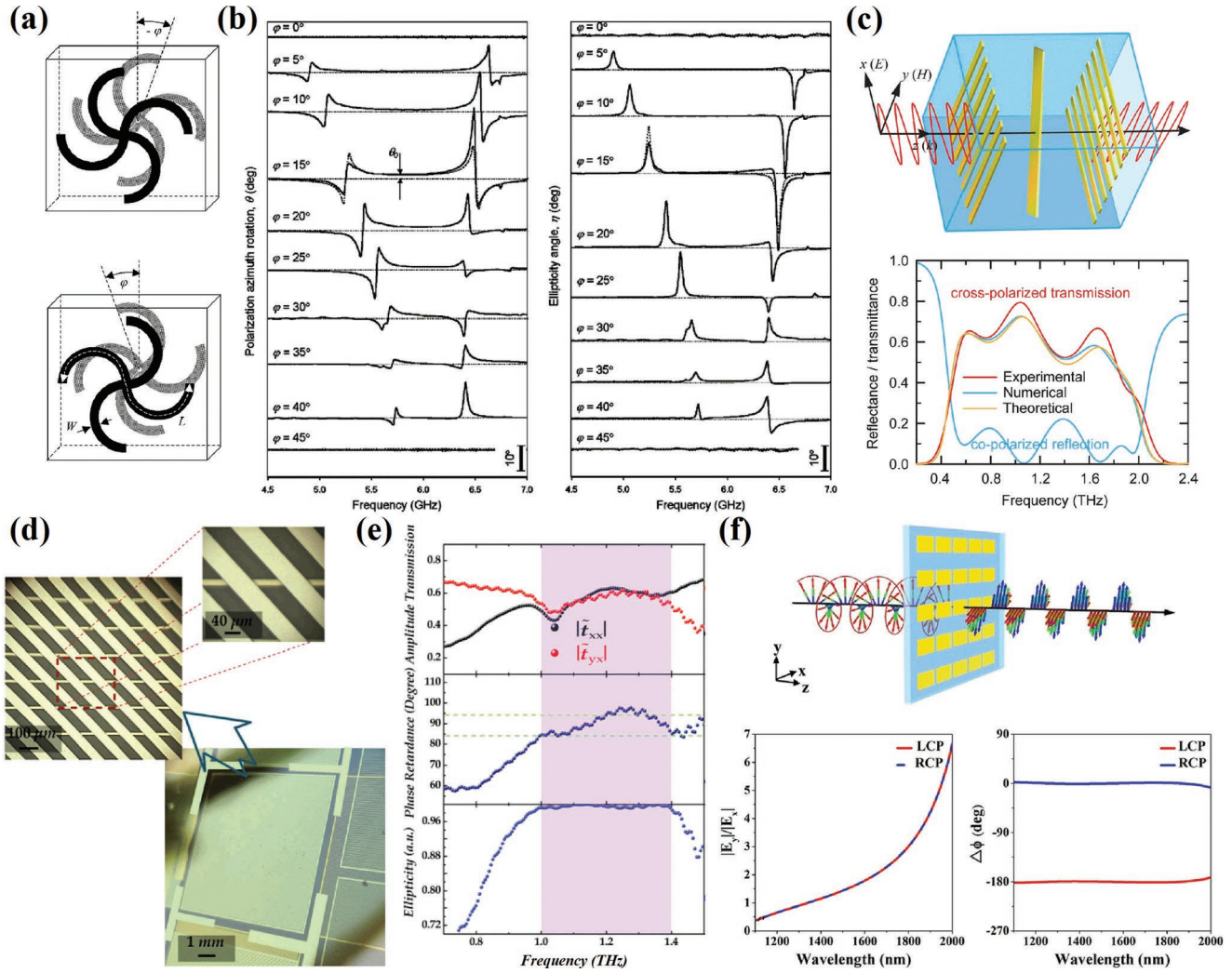

Figure 5. Manipulation of polarization state by few-layer metasurfaces. a) Schematic of twisted rosettes with different handedness. b) Experimental results of the frequency dependent polarization azimuth rotation (left panel) and ellipticity (right panel). (a,b) Reproduced with permission.[138] Copyright 2006, APS. c) Upper panel: schematic of the meta-atom of the few-layer metasurface linear polarization converter. Lower panel: experimental, simulated, and calculated cross-polarized transmission and simulated copolarized reflectance. Reproduced with permission.[54] Copyright 2013, AAAS. d) Optical images with different levels of zooming of few-layer metasurface quarter-wave plaste. e) Amplitude transmissions and phase retardance between orthogonal components, and the corresponding calculated ellipticity for experiments. (d,e) Reproduced with permission.[147] Copyright 2014, Wiley-VCH. f) Upper panel: schematic of few-layer metasurface circular-to-linear polarization converter. Lower panel: Simulated amplitude ratio and phase difference of the electric components of the transmitted wave under LCP and RCP illuminations. Reproduced with permission.[150] Copyright 2015, NPG.

design principle, broadband dispersionless OR has been achieved when the metasurface operated in the off-resonance frequency range.[140] The metasurface is built by sandwiching a metallic mesh between two conjugated gammadion resonators. The two resonances of the metasurface are well separated, thus the off-resonance frequencies and high-dispersion OR effect can be effectively suppressed. Through ingenious designing, the two well separated resonances can independently act as a polarization rotator, hence a dual-band 90° polarization rotator has been realized based on a few-layer chiral metasurface.[141] In addition to the coupling between electric and magnetic dipoles, the magnetic dipole–dipole coupling has also been demonstrated to achieve a 90° polarization rotator.[142] The few-layer metasurface consists of four pairs of cut-wire on four sides of the square. Magnetic dipoles on the upper and lower sides of the square can be directly excited by the incidence. Strong transverse magnetic dipole coupling occurs because they are exactly the same, this coupling leads to remarkable antiparallel currents on the left and right sides, which results in strong conversion of polarization.

The other methods to manipulate the polarization state of electromagnetic waves are mainly based on multiple wave interference. To achieve a complete polarization conversion, it requires that the material has two eigenmodes with a phase difference of π at the resonance frequency in two orthogonal polarization states, theoretically. Few-layer metasurfaces can provide more degrees of freedom to modulate the eigenmodes, thus it is more likely to realize a complete polarization conversion. It has been demonstrated that single-layer L-shaped holes can rotate the linearly polarized wave to

45°.[143] By inserting a cavity between the two layers of L-shaped hole system to form a FP cavity, a further degree to modulate the eigenmodes can be provided and a nearly complete polarization conversion has been realized.[144] This result arises from the coupling between the FP resonance and plasmonic modes, which leads to the overlap between two orthogonal polarization states, hence the phase difference can be modified to a complete polarization conversion. Another strategy is using the metasurfaces as auxiliary surfaces to construct the FP cavity as shown in Figure 5c.[54] The nanorod itself can be used as a linear polarization conversion device when the incident wave is polarized at 45° with respect to its long axis. When the nanorod arrays are sandwiching between a set of orthogonal gratings, a series of reflections occurs inside the gratings, thus the energy of the incident wave interacts with the nanorods repeatedly. The lower panel of Figure 5c indicates the experimental results of the broadband high efficiency polarization conversion in transmission mode. Moreover, this interferometric mechanism is universally applicable for linear polarization devices. By replacing the nanorod with gratings oriented at 45° respect to the y axis, a nearly perfect orthogonal polarization conversion has also been demonstrated.[145] Due to the broad bandwidth characteristic of the gratings, this device can operate in ultrabroad band. Besides, any desired polarization direction can be further achieved by rotating the oriented angles of the gratings. Waveguide cavities have also been integrated with this configuration.[146] The waveguide cavities have the ability to confine the incident electromagnetic wave, and the two orthogonal slots etched at the center of the front and bottom surfaces are used to couple the energy in and out. A slot tilted 45° inserted between the two orthogonal slots was utilized to subtly transform the energy from the front cavity to the back one, as a result, a cavity-based 90° polarization rotator was realized.

Although realizing the arbitrary manipulation of the polarization state is the ultimate goal, the wave plates are still worth discussing because of their widespread applications. The main problem faced by conventional birefringent crystals is the narrow bandwidth, which is limited by the dispersive properties of the crystals. By contrast, by properly designing, few-layer metasurfaces have the ability to achieve broadband perfect wave plates. A broadband, high-efficiency, and tunable quarter-wave plate based on a few-layer metasurface has been demonstrated as exhibited in Figure 5d.[147] The quarter-wave plate was constituted of stacked metallic wire grids, the front grating is oriented at −45° with respect to the x axis while the back grating is oriented at 0°. The width of both the metal strips and the air space was increased, thus only the TM-polarized wave with an electric component perpendicular to the strips can couple to the surface plasmons (SPs), and the TE-polarized wave can transmit due to the large air space without inducing SPs. Moreover, the phase retardance caused by the briefringence of the front grating is positively related to frequency. In order to compensate the dispersion of the front grating, the back grating was designed with an increased air space and a decreased grating width, which facilitated the diffraction of the TM mode and introduced a phase retardance negatively correlated with frequency. As a result, an approximately achromatic $\pi/2$ phase retardance with high transmission is achieved as shown in Figure 5e. From the previous discussion we can get the conclusion that the core of constructing wave plates by few-layer metasurfaces is to introduce a desired phase difference between two orthogonal electric components by the front and the back layers. Following this principle, another few-layer metasurface consisted of two layers of hockey-stick-like metallic arrays, which can realize linear-to-circular polarization conversion that has been proposed as well.[148] The combined structure is similar to placing another polarizer between a set of orthogonal polarizers. Furthermore, a $\pi/2$ phase retardance is introduced between the two linearly polarized components. By tuning the phase retardance to π, high-efficiency half-wave plate can also been achieved by few-layer metasurfaces.[149] The whole nanostructure lacked C_4 symmetry, so it was anisotropic for linearly polarized electromagnetic waves, which is important for constructing half-wave plates. When the metasurface is under illumination with polarization along the slow axis, large surface currents can be induced. The excited electric and magnetic dipoles cause a large effective refractive index, while no significant electric or magnetic dipoles are excited under illumination with orthogonal polarization, leading to a small effective refractive index. As a consequence, the π phase difference between the fast and slow axes is introduced due to this large anisotropy.

Conversion of polarization can be realized by other mechanisms based on few-layer metasurfaces as well. For a single-layer metasurface deposited on the dielectric substrate, the phase of the copolarized transmitted light is limited to the $(-\pi/2, \pi/2)$ range.[19] Therefore, it is hard to realize a perfect quarter-wave plate in a periodic metasurface due to the phase difference of $\pi/2$ in the transmission coefficient T_{xx} and T_{yy} is needed. However, the range of phase of transmission coefficient can be extended by embedding the structure into the substrate as shown in the inset of Figure 5f,[150] due to the same refractive index on both sides of the nanostructures. The lower panels of Figure 5f show the simulated amplitude ratio and phase difference of the transmitted wave for RCP and LCP incidences. Moreover, since the metasurface is time reversal symmetric, the conversion of linearly polarized wave to circularly polarized one can also be realized. Cascaded tensor Huygens surface can also be used as a broadband and high-efficiency circular polarizer.[151] The high efficiency arises from the overlapping of electric and magnetic dipoles within the dielectric twisted strips, while the symmetry breaking of the few-layer metasurface leads to the different transmittances between LCP and RCP waves. For reflective MIM metasurfaces, to completely manipulate the polarization state of the reflective wave, the reflection coefficients of the orthogonal polarization are different. Electric resonances for both orthogonal polarizations can be provided by H-shaped nanoantennas, the underlying metal plate provides currents flowing opposite to the H nanoantennas, thus the entire system exhibits magnetic responses at the resonance frequencies.[152] Besides, reflective MIM metasurfaces can maximize the conversion efficiency. The inherent physics of this configuration has been further explored.[153] Due to the finite penetration length of the metal in the optical frequencies, in addition to the magnetic responses, electric responses exist simultaneously, forming a symmetric mode. Using the thickness-dependent dispersion of the dielectric layer to compensate for the intrinsic dispersion of the metallic nanoantennas, broadband wave plates have been later

proposed.[154,155] The abovementioned few-layer metasurfaces are limited to one or several polarization conversion functions once the structure is built. However, it is more inspiring to dynamically manipulate the process of polarization conversions. By integrating graphene and anisotropy metasurfaces, the graphene-loaded metasurfaces can dynamically modulate the polarization states of electromagnetic waves with a widely tunable range by electrically changing the Fermi energy of the graphene sheets.[156–158] A more straightforward strategy can be applied in terahertz range, since the few-layer metasurfaces are large enough to make mechanical manipulation possible.[159] Linearly polarized THz wave can be rotated to any direction by mechanically rotating the few-layer metasurface, which is based on three rotatable gratings.

3.3. Manipulation of Phase

Phase manipulation plays a vital role both in traditional and emerging optical devices. Numerous novel applications, such as metalenses, vortex beam generators, and metaholograms, have been realized by using the phase gradient metasurfaces over the past decades.[7,160,161] The details about the phase gradient metasurfaces can be found in several previous review articles, which have reviewed the efficiency issue of metasurfaces,[46] the physics and applications of metasurfaces,[160] and the gradient metasurfaces proposed in recent years.[161] However, with the rapid progress of modern optics and photonics, single-layer metasurfaces can no longer satisfy the growing demand in controlling the phase of electromagnetic waves. Due to the lack of magnetic resonance and the equal forward and backward scattering of the surface electric current, the phase modulation range of the copolarized transmitted light and the transmission efficiency of the cross-polarized light are fundamentally limited for single-layer ultrathin transmissive metasurfaces.[19] Although these limits can be partially resolved by using thicker dielectric structures, these structures always need relatively larger size compared with plasmonic structures and have limited degrees of freedom to control the phase. However, few-layer metasurfaces can easily realize high-efficiency transmission and cover the full 2π phase range.[20,162–164] In addition, the few-layer metasurfaces can provide more degrees of freedom to manipulate the phase. Below are some typical applications in phase manipulation with the use of few-layer metasurfaces.

3.3.1. Beam Deflector

According to Fermat's principle, if a metasurface can provide a lateral phase gradient with a subwavelength resolution along the interface, the directions of the reflection and transmission lights can be controlled at will, which are governed by the generalized Snell's laws.[10] One way to realize high-efficiency beam deflectors in transmission geometry is to use few-layer Huygens' metasurfaces, which can provide both electric and magnetic polarization currents.[40,41,165] **Figure 6**a shows a unit cell of the Huygens' surface that can realize reflectionless anomalous refraction at microwave frequencies.[40] The copper patterns on the top layer provide the electric polarization currents and the split-ring resonators on the bottom layer provide the magnetic polarization currents. The needed phase gradients are obtained by changing the geometrical parameters of the structures. It can be seen from Figure 6b that a clear anomalous refraction is realized under normally incident waves. The broadband and high-efficiency performance of this metasurface is also demonstrated in Figure 6c. This method was later applied to realize the first experimental Huygens' metasurface at optical frequencies based on cascaded metallic sheets.[41] Another kind of high-efficiency few-layer metasurface that can fully control the phase of transmitted lights is the metatransmit-array.[42] As shown in Figure 6d, the metatransmit-array consists of three stacked metasurfaces made of plasmonic and dielectric composite materials. The reactance of the building blocks can be tuned by the width of the plasmonic portion. The amplitude and phase of the transmission coefficient can be tuned by the width of the plasmonic portion in the external and internal metasurfaces, as shown in Figure 6e,f. From Figure 6g, we can see that the anomalous refraction can be realized by properly choosing and arranging eight different elements. In addition, different from some other phase manipulation methods that work on the cross-polarized light, this method operates on the same polarization of the incident light. For a reflective type metasurface, one way to realize high-efficiency phase manipulation is to utilize the gap-plasmon resonance,[8,166] which can be generated by the MIM structure. Based on this configuration, Sun et al. proposed a high-efficiency broadband anomalous reflector that can realize anomalous reflection with an efficiency up to 80% at ≈850 nm.[34] In addition, the polarization of the anomalous reflection beam can be same as the polarization of the incident beam. Recently, an ultrabroadband and highly angle-resolved anomalous reflection has been demonstrated based on this method.[166] The metasurface consists of two vertically integrated aluminum (Al) trapezoid-shaped antennae and an optically thick Al substrate. The reflected light is efficiently angle-resolved to a single diffraction order over a broad bandwidth from the visible range to the NIR range. Both the near-field coupling effects and the weak interaction effect contribute to the ultrabroadband anomalous reflection. The coupling between the lower antenna and the Al substrate dominates the gap-plasmon resonance in the NIR regime, while the coupling between the upper antenna and the lower antenna dominates the optical response in the visible regime. At the same time, the unwanted interaction between the vertically cascaded antenna arrays should be weakened to alleviate the disturbance in the same waveband. It should be noticed that although most of the few-layer metasurfaces are more thicker and more difficult to manufacture compared with single-layer metasurfaces, it is possible to realize ultrathin few-layer metasurfaces with one-step nanofabrication process that is easier than the fabrication of single-layer metasurfaces. Recently, Qin et al. proposed a hybrid bilayer metasurface that has a total thickness of only 130 nm and does not need the lift-off process.[167] As shown in Figure 6h, the metasurface is composed of a gold V-shaped nanoantenna layer and a V-shaped Babinet-inverted aperture layer, which are separated by conformal hydrogen silsesquioxane pillars. By changing the geometrical parameters and the orientation angle of the V-shaped structures, the phase of the cross-polarized transmitted light

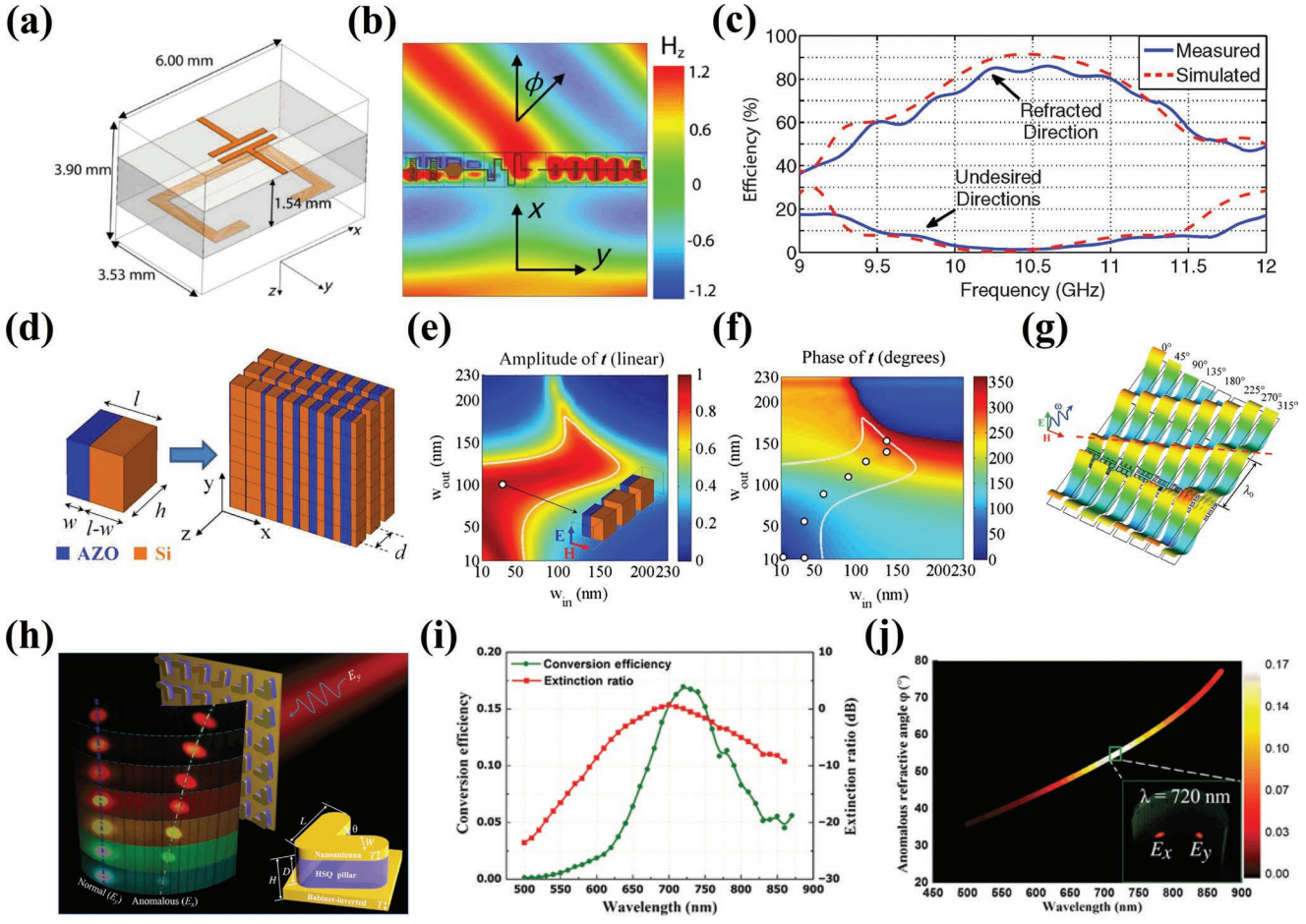

Figure 6. Beam deflector. a) Unit cell of the Huygens' surface that can realize reflectionless anomalous refraction at microwave frequencies. b) Simulated magnetic field (H_z) of the Huygens' surface for normally incident *y*-polarized plane wave. c) Measured and simulated efficiency of the Huygens' surface. (a)–(c) Reproduced with permission.[40] Copyright 2013, APS. d) Schematic of the metatransmitarray that can realize high efficiency anomalous refraction in the mid-infrared range. e) Amplitude and f) phase of the transmission coefficient as a function of the width of the plasmonic portion in the external and internal metasurfaces. g) Simulated time snapshot of the total electric field for different structures. (d)–(g) Reproduced with permission.[42] Copyright 2013, APS. h) Schematic of the high-efficiency anomalous refraction of visible light with a complementary few-layer metasurface. i) Experimental results of the conversion efficiency and extinction ratio. j) Measured transmission of anomalous light as a function of wavelength and anomalous refraction angle. (h)–(j) Reproduced with permission.[167] Copyright 2016, AAAS.

can be changed from 0 to 2π. The experimental results of the conversion efficiency, extinction ratio, and transmission of anomalous light are shown in Figure 6i,j, respectively. The near-field coupling between electric resonance on the top layer and magnetic resonance at the bottom aperture structure breaks the 25% efficiency limitation of ultrathin single-layer metasurfaces. A measured cross-polarization conversion efficiency of 17% and a simulated efficiency of 36.5% are achieved in the visible range, which are better than most of the presented single-layer plasmonic metasurfaces. Therefore, few-layer metasurfaces have the potentials to surpass the single-layer metasurfaces in beam deflectors and other applications.

3.3.2. Other Applications in Phase Manipulation

Few-layer metasurfaces can not only realize the beam deflectors, but also realize the metalenses,[63,64,168–172] vortex beam generators,[173] Bessel-beam generators,[174,175] coding metasurfaces,[176] phase holograms,[177] virtual shaping,[178] and some other phase manipulation devices. Metalenses can be designed by imposing a hyperboloidal transmission/reflection phase profile on the metasurfaces to convert incident planar wavefronts into spherical ones.[8,12] Compared with conventional refractive lenses, metalenses have many outstanding merits, such as the ultrathin and planar geometric features, the simplicity of fabrication, and the diversity of functions. These features facilitate the integration of metalenses and the miniaturization of optical imaging systems. For example, Arbabi et al. proposed a miniature optical planar camera by using a wide-angle metalens doublet.[63] Although the single-layer metasurfaces can easily realize the spherical-aberration-free focusing under normally incidence, the correcting of other monochromatic aberrations (i.e., coma and astigmatism) is still a difficult problem. However, by cascading two metasurfaces and forming a metalens doublet, the monochromatic aberrations can be well corrected.

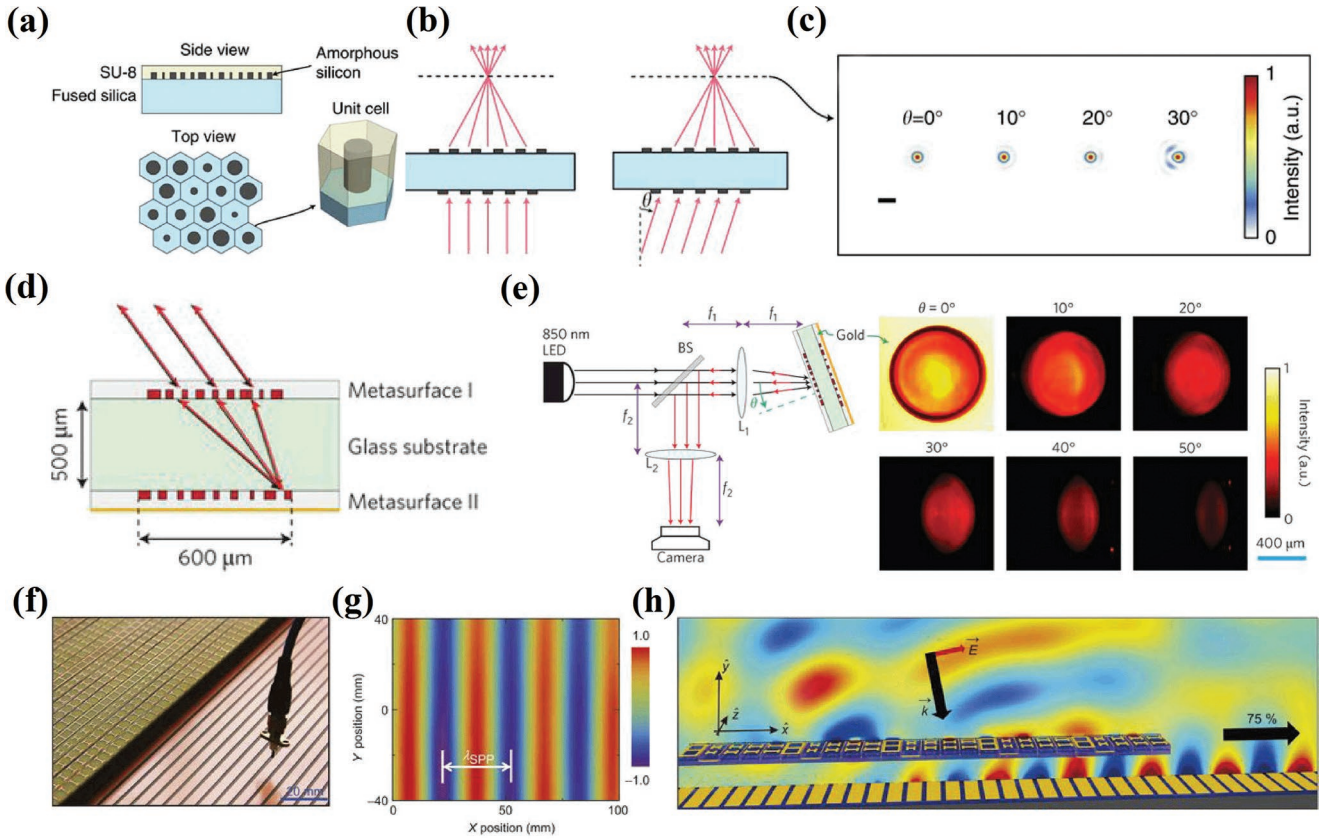

Figure 7. a) Schematics of the metasurface doublet lens. b) Schematics of focusing of on-axis and off-axis light by the metasurface doublet lens corrected for monochromatic aberrations. c) Simulated focal plane intensity for different incident angles. (a)–(c) Reproduced with permission.[63] Copyright 2016, NPG. d) Schematics of the building block of the planar retroreflector. e) Left panel: measurement set-up. Right panels: measured reflectance profiles of the retroreflector as a function of incident angles. (d,e) Reproduced with permission.[179] Copyright 2017, NPG. f) Image of the high-efficiency surface plasmon metacouplers and the monopole antenna used to probe the SPP field distribution. g) Measured Re(E_z) field distribution on part of the "plasmonic metal" when the metacoupler is illuminated by an input wave at an incident angle of $\theta_i = 8^\circ$. h) Simulated (H_y) field distribution for the device illuminated by an incident Gaussian beam at $\theta_i = 8^\circ$. (f)–(h) Reproduced with permission.[180] Copyright 2016, NPG.

Figure 7a shows the dielectric metasurface used to implement the metalens doublet. Arrays of amorphous silicon nanoposts arranged in hexagonal lattices are patterned on both sides of a fused silica substrate. The first layer and the second layer operate as a corrector plate and a focusing metasurface, respectively. Nearly diffraction limited focusing can be achieved for a wide range of angles of incidence in the NIR range, as shown in Figure 7b,c. By placing the metalens doublet on top of an image sensor, an ultraslim, low *f*-number camera that exhibits nearly diffraction limited performance over a large field of view can be realized. Soon after this work, a metalens doublet that works in the visible range was proposed.[64] This metalens is based on the principle of the Chevalier Landscape lens, and can correct the monochromatic aberrations at a wavelength of 532 nm. Few-layer metasurfaces are also suitable for designing multiwavelength or achromatic metalenses.[65,172] Recently, Zhou et al. proposed a few-layer noninteracting dielectric metasurface that can realize multiwavelength focusing at NIR wavelengths.[172] The few-layer design strategy can independently manipulate the phase at different wavelengths and provide more design space for realizing multiwavelength operation, making the design of multiwavelength metadevices more easily. By cascading different metasurfaces, many new functionalities can be achieved. Recently, Arbabi et al. proposed a planar retroreflector that can reflect light along its incident direction at different angles of incidence based on the cascaded metasurfaces,[179] as shown in Figure 7d. The retroreflector consists of two vertically integrated metasurfaces, each of which are composed of arrays of amorphous silicon nanoposts with different diameters. Different from the anomalous reflection discussed above, which needs to add a constant in-plane momentum to the incident light, the retroreflector needs to change the sign and simultaneously maintains the magnitude of the in-plane momentum for different incident angles. These requirements are fulfilled by carefully designing the phase profiles of the two metasurface layers. The first layer operates as a metalens that can focus lights with different incident angles to different points on the second metasurface. Then the second metasurface provides a spatially varying momentum to change the sign of the of the in-plane momentum for different incident angles. The measurement set-up and the measured reflectance profiles of the retroreflector are shown in Figure 7e. The measured results show that the combination of the two metasurfaces can reflect light along its incident direction with a large half power field of view of 60°. These cascaded optical systems are usually based on the weak interaction between layers, which need to quench

unwanted interaction between different functional layers. Few-layer metasurfaces can also act as metacouplers that convert free space propagating waves into surface waves.[33,180] Sun et al. demonstrated that a phase gradient metasurface with MIM structure can convert a free space propagating wave to a surface wave with nearly 100% efficiency.[33] By placing a transparent metasurface above a mushroom structure at a certain distance, a high-efficiency surface plasmon metacoupler has been achieved in the microwave regime, as shown in Figure 7f,g. The unit cell is ABA sandwich structure that can support perfect transmission under normal incidence. The measured coupling efficiency can reach about 73% due to the suppression of both decoupling and surface reflections, which is quite close to the simulated efficiency shown in Figure 7h. These designs show that, by using lithographically stacked few-layer metasurfaces, many novel and sophisticated planar optical systems that do not need postfabrication alignments are foreseeable in the future.

3.4. Multidimensional Manipulation of Electromagnetic Waves

With the development of few-layer metasurfaces, the dimensions of electromagnetic waves that a metasurface can manipulate have extended from single-dimension to multidimension. The recent advances are reviewed by Chen et al. and classified from the viewpoint of different dimensional manipulations of optical waves.[181] By simultaneously manipulating more than one property of electromagnetic waves, numerous new functions can be realized. For example, by simultaneously manipulating the phase and polarization of electromagnetic waves, a linearly/circularly polarized Gaussian beam can be converted into a vector Bessel beam,[182] as shown in **Figure 8**a. The unit cells of the Bessel beam generators consist of three anisotropic sheet admittances, which can act as a half-wave plate for the linear-to-Bessel metasurface and a quarter-wave plate for the circular-to-Bessel metasurface, respectively. This metasurface can convert the circularly polarized Gaussian beam into a radially polarized Bessel beam, as shown in Figure 8b. The measured profile of the transmitted wave front shown in Figure 8c indicates that two well shaped Bessel beams have been generated in the microwave range. Indeed, by rational phase and polarization manipulation, arbitrary vector optical fields can be achieved. Li et al. proposed a two-layer plasmonic metasurface that can simultaneously control the polarization and phase distributions of the transmitted light in the NIR range.[49] The unit cell of the metasurface consists of a pair of rectangular nanoapertures. The phase of the transmitted light can be tuned by changing the lateral translation S (shown in Figure 8d) and the aperture length L due to the waveguide mode effect. The polarization of the transmitted light is perpendicular to the major axis of the nanoaperture and can be tuned by the orientation of the rectangular nanoaperture. Due to the existence of the PB phase under circularly polarized light incidence, the rotation of the nanoapertures will introduce an additional phase. Therefore, to realize a radially polarized beam without a helical phase profile, the additional PB phase should be compensated by tuning the dimensions of the nanoapertures. Figure 8e shows the nanoaperture pairs with various dimensions and orientations that can simultaneously control light polarization and phase distributions. Based on these structures, a standard radially polarized beam in absence of helical phase has been realized. The measured far-field intensity profiles in Figure 8f confirmed the generation of radially polarized beam. Besides the simultaneous manipulation of polarization and phase, few-layer metasurfaces are also suitable for simultaneously manipulating the phase and amplitude of electromagnetic waves.[60] By combining the asymmetric transmission and the phase manipulation, Li et al. proposed a few-layer anisotropic metasurface that can simultaneously realize high-efficiency broadband asymmetric anomalous refraction and reflection.[183] The unit cell of the metasurface exhibits a C_2 symmetry with respect to the z axis and a mirror symmetry perpendicular to the z-axis, as shown in Figure 8g. This special symmetry can realize the desired circular polarization conversion and asymmetric transmission. The multiple wave interference effect between three nanorod layers and SiO_2/air interface greatly enhanced the polarization conversion efficiency and the asymmetric transmission efficiency. By utilizing the PB phase, the metasurface can realize asymmetric anomalous reflection and refraction for circularly polarized light, as shown in Figure 8h. Moreover, for linearly polarized light propagating along forward/backward direction, it will be converted into two anomalous LCP/RCP waves propagating in opposite directions. These works indicate that few-layer metasurfaces may find numerous opportunities in multidimensional manipulation of electromagnetic waves. The polarization, amplitude, phase, and even frequency of electromagnetic waves may be simultaneously manipulated in the future, which will bring out plenty of novel applications.

3.5. Multifunctional Few-Layer Metasurfaces

Most of the few-layer metasurfaces we have discussed can only achieve a single functionality. With the development of modern photonics, optical devices capable of achieving multiple functionalities are desired. Therefore, multifunctional metasurfaces have become a new research hotspot in recent years.[184–186] Compared with single-layer metasurfaces, few-layer metasurfaces can provide more degrees of freedom through strong or weak interactions between layers. Therefore, it is easier to implement polarization-dependent functionalities or multiple functionalities at different wavelengths.

We will first discuss multifunctional few-layer metasurfaces based on near-field coupling effects. Usually several layers of nanostructure form a complete functional meta-atom in this type of few-layer metasurfaces, which can easily realize polarization-dependent multiple functionalities. The most intuitive idea to achieve polarization dependence is to introduce anisotropic meta-atoms. By selecting the appropriate nanoantennas and arranging them reasonably, different phase gradients can be achieved independently for x- and y-polarized waves. As an example, incident waves with x-polarization can be converted into SPPs while the y-polarized waves can be focused.[187] Besides, the SPP waves can be excited at desired interfaces by tuning the wavelength of incidence due to the satisfaction of different Kerker condition. Most metasurfaces work only in reflection or transmission mode, leaving half of the space unused. A specifically designed metasurface which

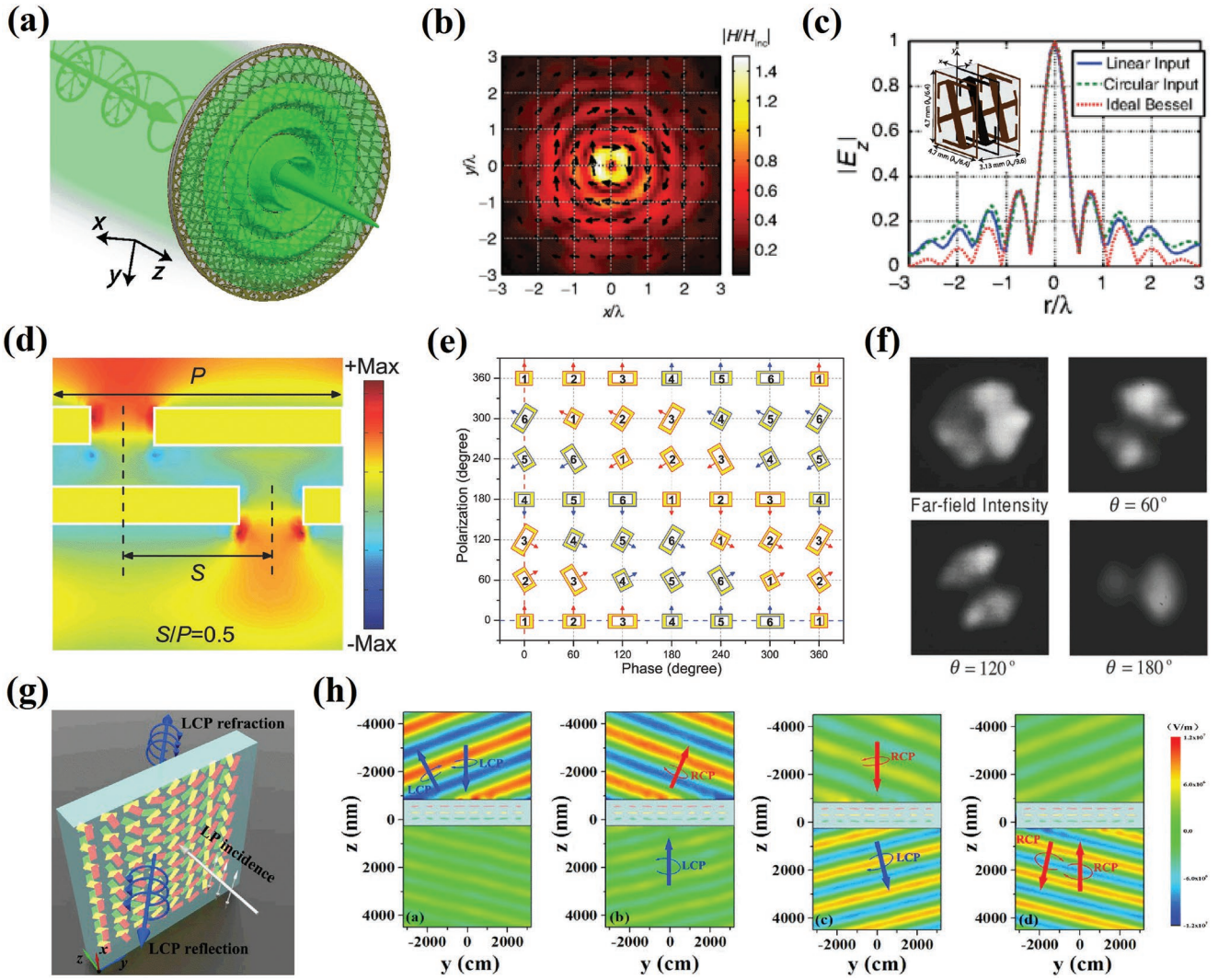

Figure 8. Multidimensional joint manipulation of electromagnetic waves. a) Schematics of the anisotropic metasurface that can transform a circularly polarized Gaussian beam into a vector Bessel beam. b) Measured transmitted magnetic field in the *xy* plane when a LCP Gaussian beams is incident on the circular-to-Bessel metasurface. c) Measured profile of the transmitted wave front. Inset shows a unit cell of the metasurfaces. (a)–(c) Reproduced with permission.[182] Copyright 2014, APS. d) Simulated E_y field distribution for the laterally translated nanoapertures in the *y*–*z* plane. e) Schematics of the nanoaperture pairs with various dimensions and orientations that can simultaneously control light polarization and phase distributions. f) Measured far-field intensity profiles of the generated radially polarized beam without and with a polarizer (oriented at angle θ) intercepted before the CCD camera. (d)–(f) Reproduced with permission.[49] Copyright 2015, Wiley-VCH. g) Schematics of the metasurface that can simultaneously generate asymmetric anomalous refraction and reflection waves. h) Simulated electric field distributions for LCP (left) and RCP (right) normal incident waves propagating along forward and backward directions, respectively. (g,h) Reproduced with permission.[183] Copyright 2016, NPG.

can manipulate polarization-dependent reflective and transmissive wave fronts was proposed recently as shown in **Figure 9**a. Therefore, the manipulation of electromagnetic waves has been upgraded to the full space.[188–190] For a mirror-symmetric meta-atom, in order to achieve independent control of reflection and transmission, it is necessary to make the meta-atom completely reflect *x*-polarized waves and transmit *y*-polarized waves. The meta-atom as shown in Figure 9a consists of four layers. The bottom two continuous metallic strips serve as gratings to allow only *y*-polarized waves passing while the upper two layers of anisotropic metallic crosses can tune the phases of reflected and transmitted waves. The reflection phase of the *x*-polarized waves is tuned by the magnetic resonances generated by the coupling between the upper resonators and bottom stripes, and the transmission phase of the *y*-polarized waves is manipulated by adjusting the geometrical parameters of the *y*-orientated bars in the four layers because Lorentz resonances of the short bars are much higher than the working frequency of the few-layer metasurface. Thus, the independent controls of both reflected and transmitted waves are achieved as shown in Figure 9b, and different bifunctional metadevices operating in full space have been demonstrated latter. Based on this structure, optical vortices with different topological charges have also been generated at both reflection/transmission sides of the metasurface.[191] The bifunctional metasurfaces have been further extended to trifunctional metasurfaces.[192] The main difference is that the

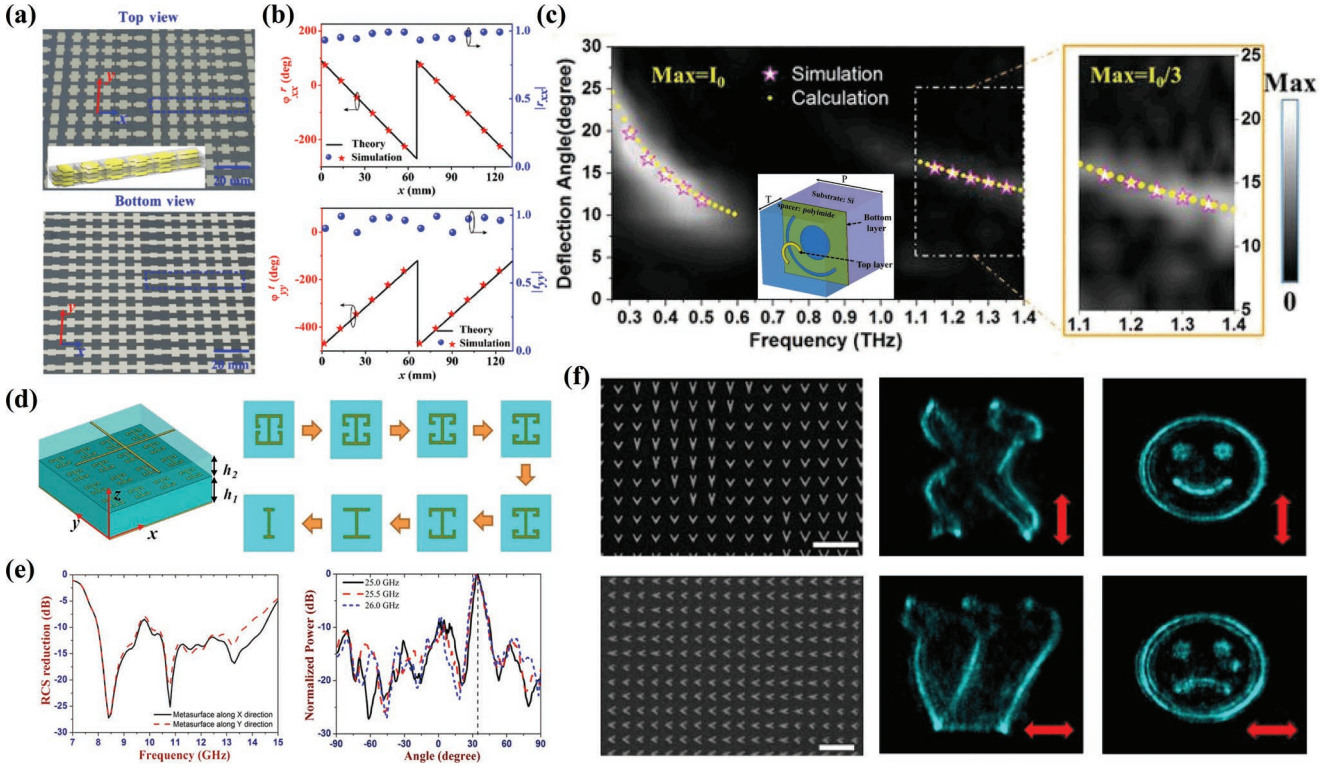

Figure 9. Multifunctional few-layer metasurfaces. a) Top-view and bottom-view pictures of the fabricated full-space beam deflector. b) Simulated reflection and transmission amplitudes and phases of the meta-atom, compared with the theoretically requested lines. (a,b) Reproduced with permission.[188] Copyright 2017, APS. c) Experimental results of the deflection effect, simulated and calculated results are plotted as pink pentagrams and yellow dots, respectively. Inset: Schematic of a meta-atom for the dual-wavelength achromatic metasurface. Reproduced with permission.[60] Copyright 2016, NPG. d) Schematic of multifunctional few-layer metasurface and topological morphing route of the lower layer to achieve different phase retardance. e) Experimental results of an obvious RCS reduction in the wide band and a deflection effect at 25 GHz. (d,e) Reproduced with permission.[194] Copyright 2016, NPG. f) SEM images of the fabricated few-layer metasurface and different holographic images under vertically (upper panel) and horizontally (lower panel) polarized illuminations. Reproduced with permission.[197] Copyright 2016, NPG.

meta-atom of trifunctional metasurfaces consists of five layers. The metallic grating is sandwiching between two sets of anisotropic metallic nanoantennas, thus the reflection of forward and backward *x*-polarized incident waves can be endowed with different functionalities. In addition to the few-layer metasurfaces discussed above, in which several layers of nanostructure form a complete functional meta-atom, the working bandwidth and freedoms to engineer the phase slope of single-layer metasurface can be further extended by adding another resonator due to the split resonances.[193]

When the coupling between layers is weak, few-layer metasurfaces can be designed to realize multiple functionalities at different wavelengths. However, it is hard to achieve the required amplitude and phase profiles for all working frequencies by simply combining two meta-atoms into a new one because the strong interaction still exists. Thus, the key step is to degrade the properties of one resonator by another resonator, as shown in Figure 9c.[60] The circular hole on the bottom layer plays an important role that it can weaken the coupling strength between the two layers, so that the upper and lower layers can almost independently control the functionalities at two wavelengths. A dual-wavelength achromatic deflector has been demonstrated based on this structure. It can be seen from the experimental results that the normal incidences at 0.4 and 1.25 THz have been deflected to almost the same angle. This design has been later extended to achieve two independent functionalities at different frequencies at reflection and transmission modes.[61] The circular hole on the bottom layer is replaced by an elliptical one, which can provide more degrees of freedom to tune the phase and amplitude responses for both frequencies. Weak interaction can also be realized when the size difference between the nanostructures of upper and lower layers is large. A meta-atom is shown in Figure 9d. The upper structure is cross-line nanoantenna to generate 0 and π phases, and the lower layer is a 4×4 array of I-type nanoantennas to construct a phase gradient.[194] The parameter variation of the upper cross-line nanoantennas has almost no influence on the phase gradient of the lower layer I-type structures at 25 GHz, and the upper cross-line structures have a stable phase difference of π in a wide range (8–15 GHz). Therefore, at 25 GHz, the incident wave is deflected by the lower structures to a specified direction, while an obvious radar cross-section (RCS) reduction is realized by the upper structures in the wide band as shown in Figure 9e. The upper nanoantennas can also achieve a phase gradient when more geometric parameters are considered, thus the independent and complete manipulation of the electromagnetic waves can be realized at two wavelengths. Based on this few-layer metasurface, a dual-wavelength carpet cloak has been

demonstrated.[195] The carpet cloak has the ability to mimic scattering wave from a metallic flat plate to achieve the stealth function. The coupling between the layers can also be suppressed by properly selecting the different constituent materials and the geometric parameters of the resonators on multiple layers.[196] Besides, this strategy has been further generalized to the nonlinear conversion process, as shown in Figure 9f.[197] By embedding different holograms in each layer, desired holographic images can be excited under vertically or horizontally polarized linear incidence. Different from the few-layer metasurfaces discussed above which mainly exist with strong or weak interactions between layers, the two interactions can also exist simultaneously to form a dual-band perfect absorber.[62] The metasurface is composed of a Helmholtz resonance cavity and an array of gold rings. The absorption peak at higher frequency is generated by the localized surface plasmons resonance due to the strong coupling between the Helmholtz resonance cavity and gold rings, while the other absorption peak is mainly governed by the Helmholtz resonance cavity as the electric field energy is confined around the slit of the cavity.

4. Conclusions and Outlook

To summarize, we have reviewed recent developments regarding few-layer metasurfaces. Starting from the different underlying layer effects, an overview of the manipulation of electromagnetic waves with few-layer metasurfaces has been discussed. Due to the fact that more degrees of freedom can be provided within the few-layer system, novel functionalities and phenomena have emerged compared with single-layer metasurfaces. On the other hand, few-layer metasurfaces can be fabricated in an easier way than metamaterials, thus they are more practical to play a role in both improvement of traditional-functional optical-device and development of novel-functional integral-system. With the rapid development of this research field, many novel applications and branches have appeared in the past few years. Before concluding this review, we wish to emphasize several promising research directions among the new emerging branches, based on our own perspectives:

(1) Integrated few-layer metasurfaces: In spite of few-layer metasurfaces can perform a variety of novel functionalities, most of the them at the present stage are more like separate optical devices. Actually, the need of integrated and on-chip systems is more urgent in practice.[198] Although integrated systems are more likely to be implemented by few-layer metasurfaces compared with single-layer metasurfaces, integrated design is still challenging to overcome the barriers of component compatibility and fabrication techniques. Encouraging progress has been made in integrated lenses recently. A minimized camera with total size of 1.6 mm × 1.6 mm × 1.7 mm has been achieved and can be extended as a tunable lens based on microelectromechanical systems.[60,199] With the further development of integrated few-layer metasurfaces, they can enter the practical stage like integrated circuits.
(2) Giant nonlinear few-layer metasurfaces: Although metasurfaces can provide unprecedented manipulation over nonlinear generation processes, including amplitude, polarization, and phase, the nonlinear signal generated by single-layer metasurfaces is still very weak.[200,201] The reason is that the interaction length between light and nanostructures is too short due to the ultrathin size of the single-layer metasurfaces. Few-layer metasurfaces, on the other hand, can increase the interaction length between light and nanostructures and independently tune different optical modes at nanoscale, thus having the ability to effectively improve the conversion efficiency of nonlinear processes.[202,203] Another method is to imitate the conventional quasi-phase matching process, which greatly enhances the nonlinear conversion efficiency by placing the orientation of each layer of nanostructures reasonably.[204]
(3) Biosensing based on few-layer metasurfaces: Optical sensing technology has important application prospects in medical research and pathological diagnostics, especially in detecting small numbers of molecules in highly diluted solutions. Plasmonic biosensors that can provide real-time detection of biomolecules are more valuable in clinical diagnoses and evaluations.[205,206] It has been demonstrated that ultralow-molecular-weight biomolecules at ultralow concentration can be detected by a novel plasmonic biosensor consisting of gold diffraction gratings and a metal-dielectric stack-based hyperbolic metamaterial.[207,208] The extreme biosensing sensitivity is accomplished by exciting the high-wavevector propagating modes of hyperbolic metamaterials. This layered configuration is also possible with few-layer metasurfaces for a more compact biosensing metadevice.

Acknowledgements

This work was supported by the National Key Research and Development Program of China (Grant Nos. 2016YFA0301102 and 2017YFA0303800), the National Natural Science Foundation of China (Grant Nos. 91856101, 11774186, and 11574163), the Natural Science Foundation of Tianjin for Distinguished Young Scientists (Grant No. 18JCJQJC45700), the Natural Science Foundation of Tianjin (Grant No. 16JCQNJC01700), and the 111 Project (Grant No. B07013).

Conflict of Interest

The authors declare no conflict of interest.

Keywords

few-layer metasurfaces, flat optical elements, interference, near-field coupling, resonance

Received: October 29, 2018
Revised: February 21, 2019
Published online:

[1] N. I. Zheludev, *Science* **2010**, *328*, 582.
[2] Y. Liu, X. Zhang, *Chem. Soc. Rev.* **2011**, *40*, 2494.
[3] R. A. Shelby, D. R. Smith, S. Schultz, *Science* **2001**, *292*, 77.
[4] J. B. Pendry, D. Schurig, D. R. Smith, *Science* **2006**, *312*, 1780.
[5] P. Moitra, Y. Yang, Z. Anderson, I. I. Kravchenko, D. P. Briggs, J. Valentine, *Nat. Photonics* **2013**, *7*, 791.

[6] N. Yu, F. Capasso, *Nat. Mater.* **2014**, *13*, 139.
[7] S. Chen, Z. Li, Y. Zhang, H. Cheng, J. Tian, *Adv. Opt. Mater.* **2018**, *6*, 1800104.
[8] H.-H. Hsiao, C. H. Chu, D. P. Tsai, *Small Methods* **2017**, *1*, 1600064.
[9] W. Liu, S. Chen, Z. Li, H. Cheng, P. Yu, J. Li, J. Tian, *Opt. Lett.* **2015**, *40*, 3185.
[10] N. Yu, P. Genevet, M. A. Kats, F. Aieta, J.-P. Tetienne, F. Capasso, Z. Gaburro, *Science* **2011**, *334*, 333.
[11] Z. Liu, Z. Li, Z. Liu, J. Li, H. Cheng, P. Yu, W. Liu, C. Tang, C. Gu, J. Li, S. Chen, J. Tian, *Adv. Funct. Mater.* **2015**, *25*, 5428.
[12] M. Khorasaninejad, F. Capasso, *Science* **2017**, *358*, eaam8100.
[13] W. Liu, Z. Li, H. Cheng, C. Tang, J. Li, S. Zhang, S. Chen, J. Tian, *Adv. Mater.* **2018**, *30*, 1706368.
[14] W. Wan, J. Gao, X. Yang, *Adv. Opt. Mater.* **2017**, *5*, 1700541.
[15] S. Liu, T. J. Cui, *Adv. Opt. Mater.* **2017**, *5*, 1700624.
[16] B. Yang, W. Liu, Z. Li, H. Cheng, S. Chen, J. Tian, *Adv. Opt. Mater.* **2018**, *6*, 1701009.
[17] T. Lee, J. Jang, H. Jeong, J. Rho, *Nano Convergence* **2018**, *5*, 1.
[18] Z. Li, W. Liu, Z. Li, C. Tang, H. Cheng, J. Li, X. Chen, S. Chen, J. Tian, *Laser Photonics Rev.* **2018**, *12*, 1800164.
[19] A. Arbabi, A. Faraon, *Sci. Rep.* **2017**, *7*, 43722.
[20] H. Cheng, Z. Liu, S. Chen, J. Tian, *Adv. Mater.* **2015**, *27*, 5410.
[21] C. Menzel, C. Rockstuhl, F. Lederer, *Phys. Rev. A* **2010**, *82*, 053811.
[22] B. Xie, K. Tang, H. Cheng, Z. Liu, S. Chen, J. Tian, *Adv. Mater.* **2017**, *29*, 1603507.
[23] B. Xie, H. Cheng, K. Tang, Z. Liu, S. Chen, J. Tian, *Phys. Rev. Appl.* **2017**, *7*, 024010.
[24] J. Lu, C. Qiu, W. Deng, X. Huang, F. Li, F. Zhang, S. Chen, Z. Liu, *Phys. Rev. Lett.* **2018**, *120*, 116802.
[25] F. Hao, Y. Sonnefraud, P. V. Dorpe, S. A. Maier, N. J. Halas, P. Nordlander, *Nano Lett.* **2008**, *8*, 3983.
[26] Y. H. Fu, J. B. Zhang, Y. F. Yu, B. Luk'yanchuk, *ACS Nano* **2012**, *6*, 5130.
[27] Z. Li, W. Liu, Z. Li, H. Cheng, S. Chen, J. Tian, *Opt. Lett.* **2017**, *42*, 3117.
[28] Z. Wang, F. Cheng, T. Winsor, Y. Liu, *Nanotechnology* **2016**, *27*, 412001.
[29] M. Qiu, L. Zhang, Z. Tang, W. Jin, C.-W. Qiu, D. Y. Lei, *Adv. Funct. Mater.* **2018**, *28*, 1803147.
[30] S. Zhang, Y.-S. Park, J. Li, X. Lu, W. Zhang, X. Zhang, *Phys. Rev. Lett.* **2009**, *102*, 023901.
[31] Y. Svirko, N. Zheludev, M. Osipov, *Appl. Phys. Lett.* **2001**, *78*, 498.
[32] B. Auguié, J. L. Alonso-Gómez, A. Guerrero-Martínez, L. M. Liz-Marzán, *J. Phys. Chem. Lett.* **2011**, *2*, 846.
[33] S. Sun, Q. He, S. Xiao, Q. Xu, X. Li, L. Zhou, *Nat. Mater.* **2012**, *11*, 426.
[34] S. Sun, K.-Y. Yang, C.-M. Wang, T.-K. Juan, W. T. Chen, C. Y. Liao, Q. He, S. Xiao, W.-T. Kung, G.-Y. Guo, L. Zhou, D. P. Tsai, *Nano Lett.* **2012**, *12*, 6223.
[35] X. Li, S. Xiao, B. Cai, Q. He, T. J. Cui, L. Zhou, *Opt. Lett.* **2012**, *37*, 4940.
[36] F. Ding, Z. Wang, S. He, V. M. Shalaev, A. V. Kildishev, *ACS Nano* **2015**, *9*, 4111.
[37] H.-X. Xu, S. Ma, X. Ling, X.-K. Zhang, S. Tang, T. Cai, S. Sun, Q. He, L. Zhou, *ACS Photonics* **2018**, *5*, 1691.
[38] C. Qu, S. Ma, J. Hao, M. Qiu, X. Li, S. Xiao, Z. Miao, N. Dai, Q. He, S. Sun, L. Zhou, *Phys. Rev. Lett.* **2015**, *115*, 235503.
[39] H. Cheng, S. Chen, H. Yang, J. Li, X. An, C. Gu, J. Tian, *J. Opt.* **2012**, *14*, 085102.
[40] C. Pfeiffer, A. Grbic, *Phys. Rev. Lett.* **2013**, *110*, 197401.
[41] C. Pfeiffer, N. K. Emani, A. M. Shaltout, A. Boltasseva, V. M. Shalaev, A. Grbic, *Nano Lett.* **2014**, *14*, 2491.
[42] F. Monticone, N. M. Estakhri, A. Alù, *Phys. Rev. Lett.* **2013**, *110*, 203903.
[43] L. Zhou, W. Wen, C. T. Chan, P. Sheng, *Phys. Rev. Lett.* **2005**, *94*, 243905.
[44] I. R. Hooper, T. W. Preist, J. R. Sambles, *Phys. Rev. Lett.* **2006**, *97*, 053902.
[45] W. Sun, Q. He, J. Hao, L. Zhou, *Opt. Lett.* **2011**, *36*, 927.
[46] Q. He, S. Sun, S. Xiao, L. Zhou, *Adv. Opt. Mater.* **2018**, *6*, 1800415.
[47] W. Luo, S. Xiao, Q. He, S. Sun, L. Zhou, *Adv. Opt. Mater.* **2015**, *3*, 1102.
[48] J. Duan, H. Guo, S. Dong, T. Cai, W. Luo, Z. Liang, Q. He, L. Zhou, S. Sun, *Sci. Rep.* **2017**, *7*, 1354.
[49] J. Li, S. Chen, H. Yang, J. Li, P. Yu, H. Cheng, C. Gu, H.-T. Chen, J. Tian, *Adv. Funct. Mater.* **2015**, *25*, 704.
[50] P. Yu, S. Chen, J. Li, H. Cheng, Z. Li, W. Liu, B. Xie, Z. Liu, J. Tian, *Opt. Lett.* **2015**, *40*, 3229.
[51] J. Li, P. Yu, C. Tang, H. Cheng, J. Li, S. Chen, J. Tian, *Adv. Opt. Mater.* **2017**, *5*, 1700152.
[52] H.-T. Chen, J. Zhou, J. F. O'Hara, F. Chen, A. K. Azad, A. J. Taylor, *Phys. Rev. Lett.* **2010**, *105*, 073901.
[53] L. Huang, C.-C. Chang, B. Zeng, J. Nogan, S.-N. Luo, A. J. Taylor, A. K. Azad, H.-T. Chen, *ACS Photonics* **2017**, *4*, 2111.
[54] N. K. Grady, J. E. Heyes, D. R. Chowdhury, Y. Zeng, M. T. Reiten, A. K. Azad, A. J. Taylor, D. A. Dalvit, H.-T. Chen, *Science* **2013**, *340*, 1304.
[55] J. Liu, Z. Li, W. Liu, H. Cheng, S. Chen, J. Tian, *Adv. Opt. Mater.* **2016**, *4*, 2028.
[56] H. Zhao, X. Wang, J. He, J. Guo, J. Ye, Q. Kan, Y. Zhang, *Sci. Rep.* **2017**, *7*, 17882.
[57] H.-T. Chen, *Opt. Express* **2012**, *20*, 7165.
[58] C. Menzel, J. Sperrhake, T. Pertsch, *Phys. Rev. A* **2016**, *93*, 063832.
[59] C. Liu, Y. Bai, Q. Zhao, Y. Yang, H. Chen, J. Zhou, L. Qiao, *Sci. Rep.* **2016**, *6*, 34819.
[60] J. Ding, N. Xu, H. Ren, Y. Lin, W. Zhang, H. Zhang, *Sci. Rep.* **2016**, *6*, 34020.
[61] X. Wang, J. Ding, B. Zheng, S. An, G. Zhai, H. Zhang, *Sci. Rep.* **2018**, *8*, 1876.
[62] C. Zhang, C. Huang, M. Pu, J. Song, Z. Zhao, X. Wu, X. Luo, *Sci. Rep.* **2017**, *7*, 5652.
[63] A. Arbabi, E. Arbabi, S. M. Kamali, Y. Horie, S. Han, A. Faraon, *Nat. Commun.* **2016**, *7*, 13682.
[64] B. Groever, W. T. Chen, F. Capasso, *Nano Lett.* **2017**, *17*, 4902.
[65] O. Avayu, E. Almeida, Y. Prior, T. Ellenbogen, *Nat. Commun.* **2017**, *8*, 14992.
[66] C. Menzel, C. Helgert, C. Rockstuhl, E.-B. Kley, A. Tunnermann, T. Pertsch, F. Lederer, *Phys. Rev. Lett.* **2010**, *104*, 253902.
[67] M. Mutlu, A. E. Akosman, A. E. Serebryannikov, E. Ozbay, *Phys. Rev. Lett.* **2012**, *108*, 213905.
[68] C. Huang, Y. Feng, J. Zhao, Z. Wang, T. Jiang, *Phys. Rev. B* **2012**, *85*, 195131.
[69] M. Mutlu, A. E. Akosman, A. E. Serebryannikov, E. Ozbay, *Opt. Express* **2011**, *19*, 14290.
[70] C. Pfeiffer, C. Zhang, V. Ray, L. J. Guo, A. Grbic, *Phys. Rev. Lett.* **2014**, *113*, 023902.
[71] Z. Li, S. Chen, C. Tang, W. Liu, H. Cheng, Z. Liu, J. Li, P. Yu, B. Xie, Z. Liu, J. Li, J. Tian, *Appl. Phys. Lett.* **2014**, *105*, 201103.
[72] Z. H. Zhu, K. Liu, W. Xu, Z. Luo, C. C. Guo, B. Yang, T. Ma, X. D. Yuan, W. M. Ye, *Opt. Lett.* **2012**, *37*, 4008.
[73] J. H. Shi, H. F. Ma, C. Y. Guan, Z. P. Wang, T. J. Cui, *Phys. Rev. B* **2014**, *89*, 165128.
[74] Z. Li, S. Chen, W. Liu, H. Cheng, Z. Liu, J. Li, P. Yu, B. Xie, J. Tian, *Plasmonics* **2015**, *10*, 1703.
[75] C. Zhang, C. Pfeiffer, T. Jang, V. Ray, M. Junda, P. Uprety, N. Podraza, A. Grbic, L. J. Guo, *Laser Photonics Rev.* **2016**, *10*, 791.
[76] X.-J. Shang, X. Zhai, L.-L. Wang, M.-D. He, Q. Li, X. Luo, H.-G. Duan, *Appl. Phys. Express* **2017**, *10*, 052602.
[77] Y. Ling, L. Huang, W. Hong, T. Liu, Y. Sun, J. Luan, G. Yuan, *Opt. Express* **2017**, *25*, 13648.

[78] T. Xu, H. J. Lezec, *Nat. Commun.* **2014**, *5*, 4141.
[79] N. Parappurath, F. Alpeggiani, L. Kuipers, E. Verhagen, *ACS Photonics* **2017**, *4*, 884.
[80] L. D. Barron, *Molecular Light Scattering and Optical Activity*, Cambridge University Press, New York **2004**.
[81] V. Saranathan, C. O. Osuji, S. G. J. Mochrie, H. Noh, S. Narayanan, A. Sandy, E. R. Dufresne, R. O. Prum, *Proc. Natl. Acad. Sci. USA* **2010**, *107*, 11676.
[82] V. Sharma, M. Crne, J. O. Park, M. Srinivasarao, *Science* **2009**, *325*, 449.
[83] M. Schäferling, *Chiral Nanophotonics*, Springer International Publishing, Switzerland **2017**.
[84] E. Plum, J. Zhou, J. Dong, V. A. Fedotov, T. Koschny, C. M. Soukoulis, N. I. Zheludev, *Phys. Rev. B* **2009**, *79*, 035407.
[85] J. Zhou, J. Dong, B. Wang, T. Koschny, M. Kafesaki, C. M. Soukoulis, *Phys. Rev. B* **2009**, *79*, 121104.
[86] Z. Li, R. Zhao, T. Koschny, M. Kafesaki, K. B. Alici, E. Colak, H. Caglayan, E. Ozbay, C. M. Soukoulis, *Appl. Phys. Lett.* **2010**, *97*, 081901.
[87] Z. Fan, A. O. Govorov, *Nano Lett.* **2010**, *10*, 2580.
[88] M. Hentschel, M. Schäferling, T. Weiss, N. Liu, H. Giessen, *Nano Lett.* **2012**, *12*, 2542.
[89] M. Hentschel, M. Schäferling, B. Metzger, H. Giessen, *Nano Lett.* **2013**, *13*, 600.
[90] V. E. Ferry, M. Hentschel, A. P. Alivisatos, *Nano Lett.* **2015**, *15*, 8336.
[91] N. Engheta, D. L. Jaggard, *IEEE Antennas Propag. Soc. Newslett.* **1988**, *30*, 6.
[92] Y. Tang, A. E. Cohen, *Phys. Rev. Lett.* **2010**, *104*, 163901.
[93] J. K. Gansel, M. Thiel, M. S. Rill, M. Decker, K. Bade, V. Saile, G. von Freymann, S. Linden, M. Wegener, *Science* **2009**, *325*, 1513.
[94] J. K. Gansel, M. Latzel, A. Frölich, J. Kaschke, M. Thiel, M. Wegener, *Appl. Phys. Lett.* **2012**, *100*, 101109.
[95] A. Radke, T. Gissibl, T. Klotzbücher, P. V. Braun, H. Giessen, *Adv. Mater.* **2011**, *23*, 3018.
[96] T.-T. Kim, S. S. Oh, H.-S. Park, R. Zhao, S.-H. Kim, W. Choi, B. Min, O. Hess, *Sci. Rep.* **2015**, *4*, 5864.
[97] R. Zhao, L. Zhang, J. Zhou, T. Koschny, C. M. Soukoulis, *Phys. Rev. B* **2011**, *83*, 035105.
[98] R. Zhao, T. Koschny, E. N. Economou, C. M. Soukoulis, *Phys. Rev. B* **2010**, *81*, 235126.
[99] M. Decker, M. W. Klein, M. Wegener, S. Linden, *Opt. Lett.* **2007**, *32*, 856.
[100] M. Decker, M. Ruther, C. E. Kriegler, J. Zhou, C. M. Soukoulis, S. Linden, M. Wegener, *Opt. Lett.* **2009**, *34*, 2501.
[101] D. H. Kwon, D. H. Werner, A. V. Kildishev, V. M. Shalaev, *Opt. Express* **2008**, *16*, 11822.
[102] E. Prodan, C. Radloff, N. J. Halas, P. Nordlander, *Science* **2003**, *302*, 419.
[103] P. Nordlander, C. Oubre, E. Prodan, K. Li, M. I. Stockman, *Nano Lett.* **2004**, *4*, 899.
[104] X. Yin, M. Schäferling, B. Metzger, H. Giessen, *Nano Lett.* **2013**, *13*, 6238.
[105] N. Liu, H. Liu, S. Zhu, H. Giessen, *Nat. Photonics* **2009**, *3*, 157.
[106] X. Xiong, W.-H. Sun, Y.-J. Bao, M. Wang, R.-W. Peng, C. Sun, X. Lu, J. Shao, Z.-F. Li, N.-B. Ming, *Phys. Rev. B* **2010**, *81*, 075119.
[107] Y. Cui, L. Kang, S. Lan, S. Rodrigues, W. Cai, *Nano Lett.* **2014**, *14*, 1021.
[108] M. Hentschel, V. E. Ferry, A. P. Alivisatos, *ACS Photonics* **2015**, *2*, 1253.
[109] Z. Li, W. Liu, H. Cheng, S. Chen, J. Tian, *Sci. Rep.* **2017**, *7*, 8204.
[110] Y. Zhao, M. A. Belkin, A. Alù, *Nat. Commun.* **2012**, *3*, 870.
[111] T. Petralli-Mallow, T. M. Wong, J. D. Byers, H. I. Yee, J. M. Hicks, *J. Phys. Chem.* **1993**, *97*, 1383.
[112] J. D. Byers, H. I. Yee, T. Petralli-Mallow, J. M. Hicks, *Phys. Rev. B* **1994**, *49*, 14643.
[113] J. J. Maki, T. Verbiest, M. Kauranen, S. V. Elshocht, A. Persoons, *J. Chem. Phys.* **1996**, *105*, 767.
[114] M. J. Huttunen, G. Bautista, M. Decker, S. Linden, M. Wegener, M. Kauranen, *Opt. Mater. Express* **2011**, *1*, 46.
[115] S. P. Rodrigues, S. Lan, L. Kang, Y. Cui, W. Cai, *Adv. Mater.* **2014**, *26*, 6157.
[116] S. Zhang, J. Zhou, Y.-S. Park, J. Rho, R. Singh, S. Nam, A. K. Azad, H.-T. Chen, X. Yin, A. J. Taylor, X. Zhang, *Nat. Commun.* **2012**, *3*, 942.
[117] X. Yin, M. Schäferling, A.-K. U. Michel, A. Tittl, M. Wuttig, T. Taubner, H. Giessen, *Nano Lett.* **2015**, *15*, 4255.
[118] S. P. Rodrigues, Y. Cui, S. Lan, L. Kang, W. Cai, *Adv. Mater.* **2015**, *27*, 1124.
[119] X. Gu, R. Bai, C. Zhang, X. R. Jin, Y. Q. Zhang, S. Zhang, Y. P. Lee, *Opt. Express* **2017**, *25*, 11778.
[120] C.-C. Chang, L. Huang, J. Nogan, H.-T. Chen, *APL Photonics* **2018**, *3*, 051602.
[121] Y. L. Loo, H. G. Wang, H. Zhang, C. K. Ong, *Opt. Express* **2016**, *24*, 20816.
[122] Y. Fan, F. Zhang, N.-H. Shen, Q. Fu, Z. Wei, H. Li, C. M. Soukoulis, *Phys. Rev. A* **2018**, *97*, 033816.
[123] A. Silva, F. Monticone, G. Castaldi, V. Galdi, A. Alù, N. Engheta, *Science* **2014**, *343*, 160.
[124] Z. Song, Q. He, S. Xiao, L. Zhou, *Appl. Phys. Lett.* **2012**, *101*, 181110.
[125] H. Guo, J. Lin, M. Qiu, J. Tian, Q. Wang, Y. Li, S. Sun, Q. He, S. Xiao, L. Zhou, *J. Phys. D: Appl. Phys.* **2018**, *51*, 074001.
[126] L.-H. Du, J. Li, Q. Liu, J.-H. Zhao, L.-G. Zhu, *Opt. Mater. Express* **2017**, *7*, 1335.
[127] Z. Li, W. Liu, H. Cheng, S. Chen, J. Tian, *Opt. Lett.* **2016**, *41*, 3142.
[128] Y. Q. Ye, Y. Jin, S. He, *J. Opt. Soc. Am. B* **2010**, *27*, 498.
[129] X. Zhang, N. Xu, K. Qu, Z. Tian, R. Singh, J. Han, G. S. Agarwal, W. Zhang, *Sci. Rep.* **2015**, *5*, 10737.
[130] J. Grant, Y. Ma, S. Saha, A. Khalid, D. R. S. Cumming, *Opt. Lett.* **2011**, *36*, 3476.
[131] Y. Zhang, W. Liu, Z. Li, H. Cheng, Y. Zhang, G. Jia, S. Chen, J. Tian, *Appl. Phys. Lett.* **2017**, *111*, 111109.
[132] P. C. Wu, C. Y. Liao, V. Savinov, T. L. Chung, W. T. Chen, Y.-W. Huang, P. R. Wu, Y.-H. Chen, A.-Q. Liu, N. I. Zheludev, D. P. Tsai, *ACS Nano* **2018**, *12*, 1920.
[133] L. Wei, Z. Xi, N. Bhattacharya, H. P. Urbach, *Optica* **2016**, *3*, 799.
[134] B. Yang, W. Liu, Z. Li, H. Cheng, D. Y. Choi, S. Chen, J. Tian, *Nano Lett.* **2019**, https://doi.org/10.1021/acs.nanolett.8b04923.
[135] E. Prati, *J. Electromagn. Waves Appl.* **2003**, *17*, 1177.
[136] M. Stalder, M. Schadt, *Opt. Lett.* **1996**, *21*, 1948.
[137] B. E. Saleh, M. C. Teich, B. R. Masters, *J. Biomed. Opt.* **2008**, *13*, 049901.
[138] A. V. Rogacheva, V. A. Fedotov, A. S. Schwanecke, N. I. Zheludev, *Phys. Rev. Lett.* **2006**, *97*, 177401.
[139] E. Plum, V. A. Fedotov, A. S. Schwanecke, N. I. Zheludev, Y. Chen, *Appl. Phys. Lett.* **2007**, *90*, 223113.
[140] K. Song, C. Ding, Z. Su, Y. Liu, C. Luo, X. Zhao, K. Bhattarai, J. Zhou, *J. Appl. Phys.* **2016**, *120*, 245102.
[141] H. Shi, A. Zhang, S. Zheng, J. Li, Y. Jiang, *Appl. Phys. Lett.* **2014**, *104*, 034102.
[142] Y. Ye, S. He, *Appl. Phys. Lett.* **2010**, *96*, 203501.
[143] T. Li, H. Liu, S.-M. Wang, X.-G. Yin, F.-M. Wang, S.-N. Zhu, X. Zhang, *Appl. Phys. Lett.* **2008**, *93*, 021110.
[144] T. Li, S. M. Wang, J. X. Cao, H. Liu, S. N. Zhu, *Appl. Phys. Lett.* **2010**, *97*, 261113.
[145] L. Cong, W. Cao, X. Zhang, Z. Tian, J. Gu, R. Singh, J. Han, W. Zhang, *Appl. Phys. Lett.* **2013**, *103*, 171107.
[146] J. Wang, Z. Shen, W. Wu, *Appl. Phys. Lett.* **2016**, *109*, 153504.
[147] L. Cong, N. Xu, J. Gu, R. Singh, J. Han, W. Zhang, *Laser Photonics Rev.* **2014**, *8*, 626.

[148] Y. Li, J. Zhang, S. Qu, J. Wang, L. Zheng, Y. Pang, Z. Xu, A. Zhang, *J. Appl. Phys.* **2015**, *117*, 044501.
[149] X. Wu, Y. Meng, L. Wang, J. Tian, S. Dai, W. Wen, *Appl. Phys. Lett.* **2016**, *108*, 183502.
[150] Z. Li, W. Liu, H. Cheng, S. Chen, J. Tian, *Sci. Rep.* **2016**, *5*, 18106.
[151] H. Jiang, W. Zhao, Y. Jiang, *Opt. Express* **2016**, *24*, 17738.
[152] J. Hao, Y. Yuan, L. Ran, T. Jiang, J. A. Kong, C. T. Chan, L. Zhou, *Phys. Rev. Lett.* **2007**, *99*, 063908.
[153] J. Hao, Q. Ren, Z. An, X. Huang, Z. Chen, M. Qiu, L. Zhou, *Phys. Rev. A* **2009**, *80*, 023807.
[154] S. Ma, X. Wang, W. Luo, S. Sun, Y. Zhang, Q. He, L. Zhou, *EPL* **2017**, *117*, 37007.
[155] S. Jiang, X. Xiong, Y. Hu, Y. Hu, G. Ma, R. Peng, C. Sun, M. Wang, *Phys. Rev. X* **2014**, *4*, 021026.
[156] X. Yu, X. Gao, W. Qiao, L. Wen, W. Yang, *IEEE Photonics Technol. Lett.* **2016**, *28*, 2399.
[157] J. Li, P. Yu, H. Cheng, W. Liu, Z. Li, B. Xie, S. Chen, J. Tian, *Adv. Opt. Mater.* **2016**, *4*, 91.
[158] Z. Miao, Q. Wu, X. Li, Q. He, K. Ding, Z. An, Y. Zhang, L. Zhou, *Phys. Rev. X* **2015**, *5*, 041027.
[159] R.-H. Fan, Y. Zhou, X.-P. Ren, R.-W. Peng, S.-C. Jiang, D.-H. Xu, X. Xiong, X.-R. Huang, M. Wang, *Adv. Mater.* **2015**, *27*, 1201.
[160] H. T. Chen, A. J. Taylor, N. Yu, *Rep. Prog. Phys.* **2016**, *79*, 076401.
[161] F. Ding, A. Pors, S. I. Bozhevolnyi, *Rep. Prog. Phys.* **2018**, *81*, 026401.
[162] C. Pfeiffer, A. Grbic, *Appl. Phys. Lett.* **2013**, *102*, 231116.
[163] C. Wang, W. Liu, Z. Li, H. Cheng, Z. Li, S. Chen, J. Tian, *Adv. Opt. Mater.* **2018**, *6*, 1701047.
[164] X. Yin, H. Zhu, H. Guo, M. Deng, T. Xu, Z. Gong, X. Li, Z. H. Hang, C. Wu, H. Li, S. Chen, L. Zhou, L. Chen, *Laser Photonics Rev.* **2018**, *12*, 1800081.
[165] S. L. Jia, X. Wan, D. Bao, Y. J. Zhao, T. J. Cui, *Laser Photonics Rev.* **2015**, *9*, 545.
[166] S. Gao, S.-S. Lee, E.-S. Kim, D.-Y. Choi, *Nanoscale* **2018**, *10*, 12453.
[167] F. Qin, L. Ding, L. Zhang, F. Monticone, C. C. Chum, J. Deng, S. Mei, Y. Li, J. Teng, M. Hong, S. Zhang, A. Alù, C.-W. Qiu, *Sci. Adv.* **2016**, *2*, e1501168.
[168] A. Forouzmand, S. Tao, S. Jafar-Zanjani, J. Cheng, M. M. Salary, H. Mosallaei, *J. Opt. Soc. Am. B* **2016**, *33*, 1411.
[169] B.-C. Lin, G.-M. Wang, T. Cai, *Appl. Phys. A* **2017**, *123*, 630.
[170] C.-C. Chang, D. Headland, D. Abbott, W. Withayachumnankul, H.-T. Chen, *Opt. Lett.* **2017**, *42*, 1867.
[171] Z. Lin, B. Groever, F. Capasso, A. W. Rodriguez, M. Lončar, *Phys. Rev. Appl.* **2018**, *9*, 044030.
[172] Y. Zhou, I. I. Kravchenko, H. Wang, J. R. Nolen, G. Gu, J. Valentine, *Nano Lett.* **2018**, *18*, 7529.
[173] W. Luo, S. Sun, H.-X. Xu, Q. He, L. Zhou, *Phys. Rev. Appl.* **2017**, *7*, 044033.
[174] S. Liu, A. Noor, L. L. Du, L. Zhang, Q. Xu, K. Luan, T. Q. Wang, Z. Tian, W. X. Tang, J. G. Han, W. L. Zhang, X. Y. Zhou, Q. Cheng, T. J. Cui, *ACS Photonics* **2016**, *3*, 1968.
[175] Z. Wang, S. Dong, W. Luo, M. Jia, Z. Liang, Q. He, S. Sun, L. Zhou, *Appl. Phys. Lett.* **2018**, *112*, 191901.
[176] Z. Shen, B. Jin, J. Zhao, Y. Feng, L. Kang, W. Xu, J. Chen, P. Wu, *Appl. Phys. Lett.* **2016**, *109*, 121103.
[177] S. Larouche, Y.-J. Tsai, T. Tyler, N. M. Jokerst, D. R. Smith, *Nat. Mater.* **2012**, *11*, 450.
[178] M. Pu, Z. Zhao, Y. Wang, X. Li, X. Ma, C. Hu, C. Wang, C. Huang, X. Luo, *Sci. Rep.* **2015**, *5*, 9822.
[179] A. Arbabi, E. Arbabi, Y. Horie, S. M. Kamali, A. Faraon, *Nat. Photonics* **2017**, *11*, 415.
[180] W. Sun, Q. He, S. Sun, L. Zhou, *Light: Sci. Appl.* **2016**, *5*, e16003.
[181] S. Chen, Z. Li, W. Liu, H. Cheng, J. Tian, *Adv. Mater.* **2019**, *31*, 1802458.
[182] C. Pfeiffer, A. Grbic, *Phys. Rev. Appl.* **2014**, *2*, 044012.
[183] Z. Li, W. Liu, H. Cheng, J. Liu, S. Chen, J. Tian, *Sci. Rep.* **2016**, *6*, 35485.
[184] E. Maguid, I. Yulevich, D. Veksler, V. Kleiner, M. L. Brongersma, E. Hasman, *Science* **2016**, *352*, 1202.
[185] N. M. Litchinitser, *Science* **2016**, *352*, 1177.
[186] D. Wen, F. Yue, M. Ardron, X. Chen, *Sci. Rep.* **2016**, *6*, 27628.
[187] Y. Ling, L. Huang, W. Hong, T. Liu, L. Jing, W. Liu, Z. Wang, *Opt. Express* **2017**, *25*, 29812.
[188] T. Cai, G. Wang, S. Tang, H. Xu, J. Duan, H. Guo, F. Guan, S. Sun, Q. He, L. Zhou, *Phys. Rev. Appl.* **2017**, *8*, 034033.
[189] Y. Zhuang, G. Wang, T. Cai, Q. Zhang, *Opt. Express* **2018**, *26*, 3594.
[190] T. Cai, S. Tang, G. Wang, H. Xu, S. Sun, Q. He, L. Zhou, *Adv. Opt. Mater.* **2017**, *5*, 1600506.
[191] S. Tang, T. Cai, G.-M. Wang, J.-G. Liang, X. Li, J. Yu, *Sci. Rep.* **2018**, *8*, 6422.
[192] W. Pan, T. Cai, S. Tang, L. Zhou, J. Dong, *Opt. Express* **2018**, *26*, 17447.
[193] H.-X. Xu, S. Tang, X. Ling, W. Luo, L. Zhou, *Ann. Phys.* **2017**, *529*, 1700045.
[194] C. Huang, W. Pan, X. Ma, X. Luo, *Sci. Rep.* **2016**, *6*, 23291.
[195] J. Yang, C. Huang, X. Wu, B. Sun, X. Luo, *Adv. Opt. Mater.* **2018**, *6*, 1800073.
[196] A. Forouzmand, H. Mosallaei, *ACS Photonics* **2018**, *5*, 1427.
[197] E. Almeida, O. Bitton, Y. Prior, *Nat. Commun.* **2016**, *7*, 12533.
[198] P. Cheben, R. Halir, J. H. Schmid, H. A. Atwater, D. R. Smith, *Nature* **2018**, *560*, 565.
[199] E. Arbabi, A. Arbabi, S. M. Kamali, Y. Horie, M. Faraji-Dana, A. Faraon, *Nat. Commun.* **2018**, *9*, 812.
[200] G. Li, S. Zhang, T. Zentgraf, *Nat. Rev. Mater.* **2017**, *2*, 17010.
[201] D. Wen, F. Yue, W. Liu, S. Chen, X. Chen, *Adv. Opt. Mater.* **2018**, *6*, 1800348.
[202] F. Wang, A. B. Martinson, H. Harutyunyan, *ACS Photonics* **2017**, *4*, 1188.
[203] S. Kruk, M. Weismann, A. Y. Bykov, E. A. Mamonov, I. A. Kolmychek, T. Murzina, N. C. Panoiu, D. N. Neshev, Y. S. Kivshar, *ACS Photonics* **2015**, *2*, 1007.
[204] N. Segal, S. Keren-Zur, N. Hendler, T. Ellenbogen, *Nat. Photonics* **2015**, *9*, 180.
[205] A. V. Kabashin, P. Evans, S. Pastkovsky, W. Hendren, G. A. Wurtz, R. Atkinson, R. Pollard, V. A. Podolskiy, A. V. Zayats, *Nat. Mater.* **2009**, *8*, 867.
[206] K. V. Sreekanth, S. Sreejith, S. Han, A. Mishra, X. Chen, H. Sun, C. T. Lim, R. Singh, *Nat. Commun.* **2018**, *9*, 369.
[207] K. V. Sreekanth, Y. Alapan, M. ElKabbash, E. Ilker, M. Hinczewski, U. A. Gurkan, A. De Luca, G. Strangi, *Nat. Mater.* **2016**, *15*, 621.
[208] K. V. Sreekanth, Y. Alapan, M. ElKabbash, A. M. Wen, E. Ilker, M. Hinczewski, U. A. Gurkan, N. F. Steinmetz, G. Strangi, *Adv. Opt. Mater.* **2016**, *4*, 1767.